DOI: 10.1002/ejic.201000444

Tris-Dioximate Cobalt(I,II,III) Clathrochelates: Stabilization of Different Oxidation and Spin States of an Encapsulated Metal Ion by Ribbed Functionalization

Yan Z. Voloshin,*[a] Oleg A. Varzatskii,[b] Valentin V. Novikov,[a] Nataly G. Strizhakova,[c] Ivan I. Vorontsov,[a] Anna V. Vologzhanina,[a] Konstantin A. Lyssenko,[a] Galina V. Romanenko,[d] Matvey V. Fedin,[d] Victor I. Ovcharenko,[d] and Yurii N. Bubnov[a]

Keywords: Cobalt complexes / Clathrochelates / Cage compounds / Ligand reactivity / Jahn–Teller distortion

Boron-capped hexachlorine-containing cobalt(II) clathrochelates were prepared by means of template condensation of dichloroglyoxime (Cl_2GmH_2) with boron-containing Lewis acids on a cobalt(II) ion matrix. The nucleophilic substitution of the reactive chlorine atoms of these macrobicyclic tris-dioximates with thiolate anions gave the hexasulfide cobalt(II) and dodecasulfide $Co^{III}Co^{II}Co^{III}$ mono- and bis-clathrochelates. The treatment of the hexachlorine-containing cobalt(II) precursors with primary aliphatic amines afforded hexaamine cobalt(III) clathrochelates. The reduction of these precursors led to the clathrochelate $[Co(Cl_2Gm)_3(BR)_2]^-$ anions, which were isolated as the salts with bulky organic cations. The relative stability of these cobalt(I) complexes accounted for a strong electronic effect of six electron-withdrawing ribbed chlorine substituents. Superconducting quantum interference device (SQUID) magnetometry, EPR, and multitemperature X-ray diffraction data showed that the cobalt(II) clathrochelates undergo gradual and incomplete $½ \leftrightarrow 3/2$ spin transition. The Jahn–Teller distortion of the low-spin encapsulated cobalt(II) ion causes its shift in the direction of one of the three chelate α-dioximate fragments. The anisotropic displacement parameters were used to estimate the ordering of the molecular species, and the superposition of two Jahn–Teller distorted structures was found in a crystal. The cyclic voltammetry (CV) data showed the influence of the substituents in α-dioximate fragments on the redox potentials of an encapsulated cobalt ion. The electron-withdrawing ribbed substituents stabilize the cobalt(I) oxidation state of this ion because of electron-density delocalization on their ribbed substituents, whereas the electron-donating amine groups stabilize the cobalt(III) oxidation state.

Introduction

Iron, ruthenium, and cobalt ions are thought to be the most efficient templates for the self-assembly of macrobicyclic tris-dioximates,[1] but only for cobalt complexes could one implement the synthesis of stable boron-capped clathrochelates by means of a tripodal cross-linking with boron-containing Lewis acids and with an encapsulated metal ion in three oxidation states [i.e. the cobalt(I), cobalt(II), and cobalt(III) ions].[1,2] This is attributed to simultaneous impact of the following factors: (i) a high stability of the electronic configurations d^6, d^7, and d^8 in a strong macrobicyclic ligand field, (ii) a high affinity of these ions to the nitrogen donor atoms of the cage ligands [according to the Pearson hard soft acid base (HSAB) principle], and (iii) the fact that the cavity size of these ligands in different conformations [from a trigonal prism (TP) for the cobalt(I) and cobalt(II) ions to a trigonal antiprism (TAP) for the cobalt(III) ion] fits that of the high-spin Co^+, the low- and high-spin Co^{2+}, and the low-spin Co^{3+} ions. In contrast, the iron and ruthenium ions form stable complexes of this type exclusively in the (2+) oxidation low-spin state.[1]

Very recently, the catalytic activity of the boron-capped cobalt tris-dioximates for hydrogen-forming reactions was found.[3] The formation of a cathodic electrocatalytic wave in solution in the presence of acids has been attributed to the $Co^{2+/+}$ redox couple; the cobalt(I) clathrochelates are catalytically active in these hydrogen-producing systems.[3] It was found earlier[4] that the substituents in chelate α-dioximate (ribbed) fragments, unlike the apical substituents in capping groups, have essential steric and electronic effects on a clathrochelate framework (in therefore, an encapsulated metal ion); and vice versa, the electronic state of this

[a] Nesmeyanov Institute of Organoelement Compounds of the Russian Academy of Sciences,
119991 Moscow, Russian Federation
Fax: +7-449-135-50-85
E-mail: voloshin@ineos.ac.ru
[b] Vernadskii Institute of General and Inorganic Chemistry of the National Academy of Sciences of Ukraine,
03680 Kiev, Ukraine
[c] Institute for Sorbtion and Problems of Endoecology of the National Academy of Sciences of Ukraine,
03680 Kiev, Ukraine
[d] International Tomography Center, the Siberian Branch of the Russian Academy of Sciences,
630090 Novosibirsk, Russia
Supporting information for this article is available on the WWW under http://dx.doi.org/10.1002/ejic.201000444.

metal ion affects the chemical, coordinative, and physicochemical properties of functionalizing substituents. In addition, the electronic state of an encapsulated metal ion determines, to a great extent, the route of functionalization reactions (i.e., the nucleophilic substitution of the reactive halogen atoms of clathrochelate precursors with different nucleophilic agents[4,5]). We analyzed in detail the influence of the electronic configuration of an encapsulated cobalt ion on nucleophilic substitution in a clathrochelate framework, and that of the nature of the ribbed functionalizing substituents on the chemical stability of clathrochelates with an encapsulated cobalt ion in different oxidation and spin states.

Results and Discussion

Synthesis of Complexes

The initial boron-capped hexachlorine-containing clathrochelates were prepared by means of template condensation on a cobalt(II) ion matrix (Scheme 1), like their iron-containing analogues.[4,5] The Co^{2+} ion is, however, a less efficient template, and the yields of the cobalt(II) precursors turned out to be significantly lower than those for the iron(II) ion. The reason is the values of the physical ionic (Shannon) radii of the template cobalt(II) ion (electronic configuration d^7, r_i = 0.79 and 0.885 Å for the low- and high-spin states of this ion in the octahedral environment, respectively) that are appreciably greater than that of the low-spin iron(II) ion (electronic configuration d^6, r_i = 0.75 Å). The six d electrons of the Fe^{2+} ion in a strong field of the clathrochelate ligand fully occupy three bonding d orbitals ($t_{2g}^6 \rightarrow e_g^4 + a_1^2$). On the other hand, a cobalt(II) ion forms square-planar macrocyclic bis-dioximates.[6] These side reactions also decrease the yields of the target clathrochelate precursors. The purification of the phenylboron-capped hexachlorine-containing cobalt(II) complex is complicated because of its extremely low solubility in organic solvents. Therefore, the solid product was repeatedly washed with a great amount of polar and apolar organic solvents (methanol, diethyl ether, and hexane). An analytically pure sample of this precursor was obtained by Soxhlet extraction with dichloromethane.

The nucleophilic substitution of the reactive chlorine atoms of the hexachlorine-containing cobalt(II) tris-dioximates obtained (Scheme 1) differ considerably from the similar reactions of the previously reported hexachlorine-containing iron(II) and ruthenium(II) precursors.[4,7] In the latter case, the synthesis of the hexaaryl- and hexaalkylsulfide clathrochelates was performed both with alkaline metal thiolates (RSH/MOR and RSH/M_2CO_3 systems) in solvents with a high donor number (e.g., DMF and 1,4-dioxane) and with a RSH/triethylamine system in the aprotonic solvents with a low donor number (e.g., CH_2C1_2 and $CHCl_3$). In the case of hexachlorine-containing cobalt(II) precursors, our attempts to use alkaline metal thiolates (C_6H_5SH/K_2CO_3 and n-C_4H_9SH/K_2CO_3 systems in 1,4-dioxane and DMF) as nucleophilic agents gave no target clathrochelates: their clathrochelate frameworks easily underwent a destruction with detachment of one of the three dioximate fragments to produce square-planar cobalt(II) dioximates. Therefore, we used a RSH/triethylamine system to obtain hexasulfide cobalt(II) clathrochelates under mild conditions of an aprotonic solvent with a low donor number (CH_2Cl_2). This system produced the corresponding thiolate anion and allowed us to avoid, to a great extent, the destruction of the clathrochelate framework. The treatment of the hexachlorine-containing cobalt(II) precursors with aliphatic amines afforded unexpected clathrochelate products. It was shown earlier[7,8] that hexachlorine-containing iron(II) and ruthenium(II) precursors in most solvents (DMF, benzene, CH_2Cl_2, 1,4-dioxane, and the corresponding amine) reacted with sterically unhindered primary aliphatic amines (*n*-butylamine and cyclohexylamine) to yield tetraamine clathrochelates with functionalizing substituents in two of the three dioximate fragments, but only trisubstituted complexes have been isolated in chloroform media.[7,8] With sterically hindered *tert*-butylamine and secondary amines (in particular, diethylamine) in solvents with a high donor number, the formation of trifunctionalized iron(II) complexes monosubstituted in all three dioximate fragments was predominant, whereas only disubstituted products were formed in chloroform media. The effect of both the solvent and the amine nature on the resulting amine iron(II) clathrochelates has been analyzed in detail.[8] In contrast to the reactions of the iron and ruthenium(II) precursors, the treament of the hexachlorine-containing cobalt(II) complexes with primary aliphatic amines (*n*-butylamine, *tert*-butylamine, and cyclohexylamine) led to hexaamine cobalt(III) clathrochelates under a wide range of reaction conditions. The formation of such complexes was observed in different solvents (e.g., DMF, 1,4-dioxane, CH_2Cl_2, and $CHCl_3$) with excess and with low molar amounts of the corresponding amine (relative to the hexachlorine-containing precursor), as well as with a $RNH_2/RNH_3^+Cl^-$ system to decrease the amine reactivity. In the case of *tert*-butylamine and CH_2C1_2 as a solvent, the solid reaction product contained mainly the tetraamine cobalt(II) clathrochelates [as it followed from the plasma desorption (PD) mass spectra]. The treatment of this product with an excess amount of *n*-butylamine in DMF gave a mixture of isomers of the hexaamine cobalt(III) clathrochelate with four *tert*-butylamine and two *n*-butylamine substituents (according to the ^1H and $^{13}C\{^1H\}$ NMR and PD mass spectra). It is evident that the initial solid was a mixture of isomers of the corresponding tetra-*tert*-butylamine-substituted clathrochelate rather than an individual compound. In the case of diethylamine as a nucleophile and DMF as a solvent, the formation of trisubstituted cobalt(III) clathrochelates was observed. The treatment of these triaminetrichlorine-containing complexes with primary aliphatic amines in DMF afforded the corresponding hexaamine cobalt(III) clathrochelates (Scheme 1).

When an excess amount of amine was added to a solution/suspension of a clathrochelate precursor in DMF under inert atmosphere or in the presence of a deficient

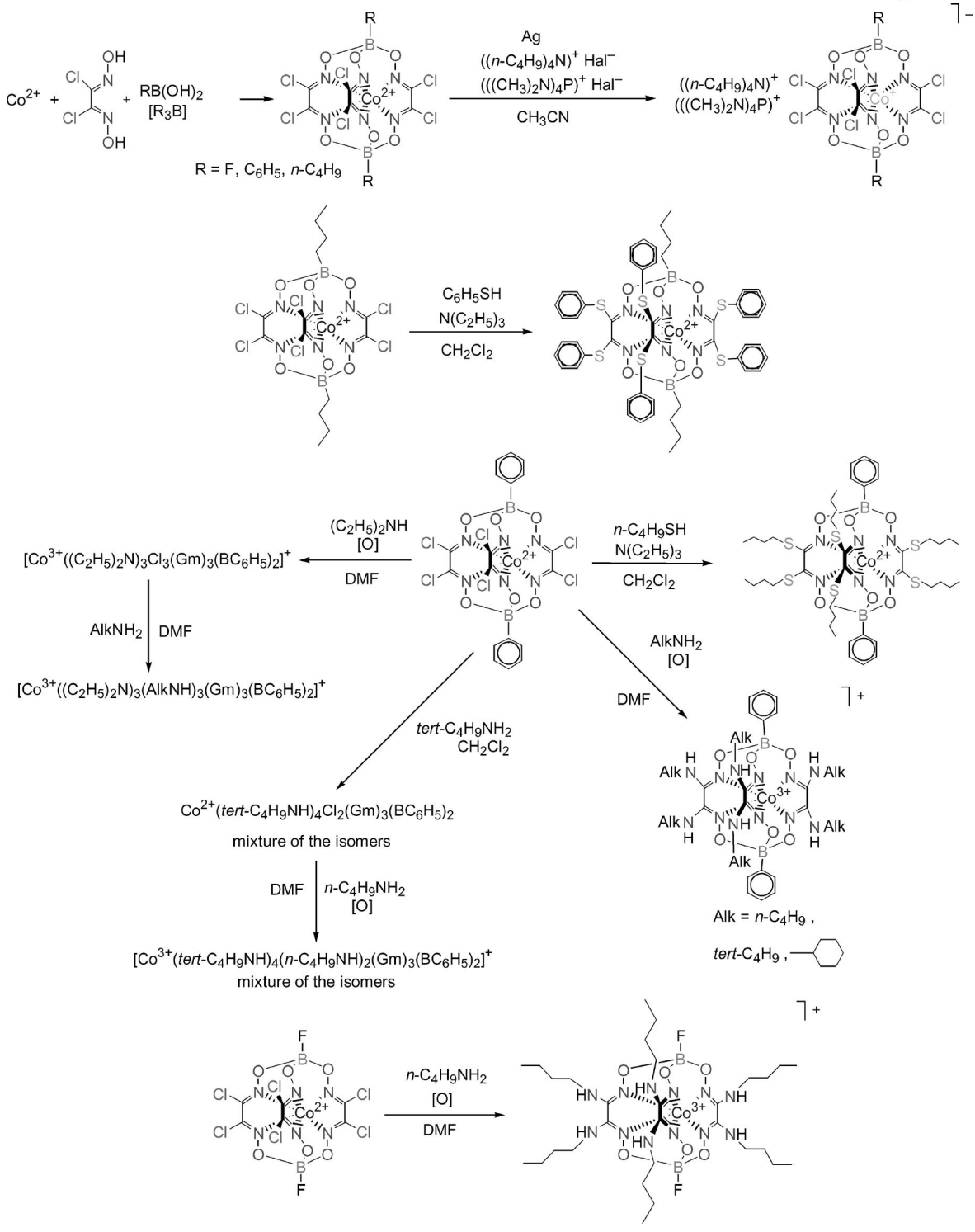

Scheme 1. Synthesis of the hexachlorine-containing clathrochelate cobalt(II) precursors, their functionalization and reduction.

amount of air oxygen, the reaction mixture became blue, then violet, and finally red-brown. Similar effects were observed in the case of the treatment of these precursors with thiolate anions: the reaction mixture acquired an intensive dark-blue coloration at the point at which a drop of organic base solution fell (i.e., when thiolate anion forms), and this blue coloration disappeared when left stirring in air. Under inert gas or in the presence of a deficient amount of air oxygen, the whole reaction mixture became blue. We assumed that this blue coloration of the reaction mixture was caused by reduction of the cobalt(II) precursor with thiolate anion to a cobalt(I) clathrochelate, thus proceeding consecutively with the nucleophilic substitution of the reactive ribbed chlorine atoms. This assumption was confirmed

by isolation of an unusual trinuclear $Co^{III}Co^{II}Co^{III}$ bis-clathrochelate as a byproduct of the treatment of $[Co(Cl_2Gm)_3(BC_6H_5)_2]$ (where Cl_2Gm^{2-} is the dichloroglyoxime dianion) with *n*-butylthiolate anion in 1,4-dioxane (Scheme 2). As clathrochelates possess both the high thermodynamical stability and low chemical reactivity[1] and the detachment of their capping fragments is extremely complicated, we proposed the following pathway for formation of this trinuclear clathrochelate: the hexachlorine-containing cobalt(II) precursor was partially reduced with a thiolate ion to produce a cobalt(I) clathrochelate, the macrobicyclic framework of which is relatively unstable because of a larger Shannon radius of the Co^+ ion than that of the Co^{2+} ion. As was mentioned above, the cavity size of a boron-capped tris-dioximate ligand is optimal for low-spin Fe^{2+} and Co^{3+} (r_i = 0.68 Å) ions, and this size coincides, to a lesser extent, with the size of the low- and high-spin Co^{2+} ions. It is evident that the high-spin Co^+ ion with electronic configuration d^8 fits this cavity to an even lesser extent. As a result, one of the two capping fragments detaches with the formation of a semiclathrochelate structure, thus revealing the rigidity of the clathrochelate framework. Then three possibilities exist. The first one is that the resulting hexachlorine-containing semiclathrochelate undergoes nucleophilic substitution with thiolate ions, then oxidation of the encapsulated cobalt ion, and the subsequent cross-linking of the molecules of hexasulfide semiclathrochelate formed with the cobalt(II) ions, which are present in the reaction mixture because of a partial destruction of the clathrochelate framework. The second one is that two molecules of the hexachlorine-containing semiclathrochelate formed were cross-linked with a cobalt(II) ion to produce

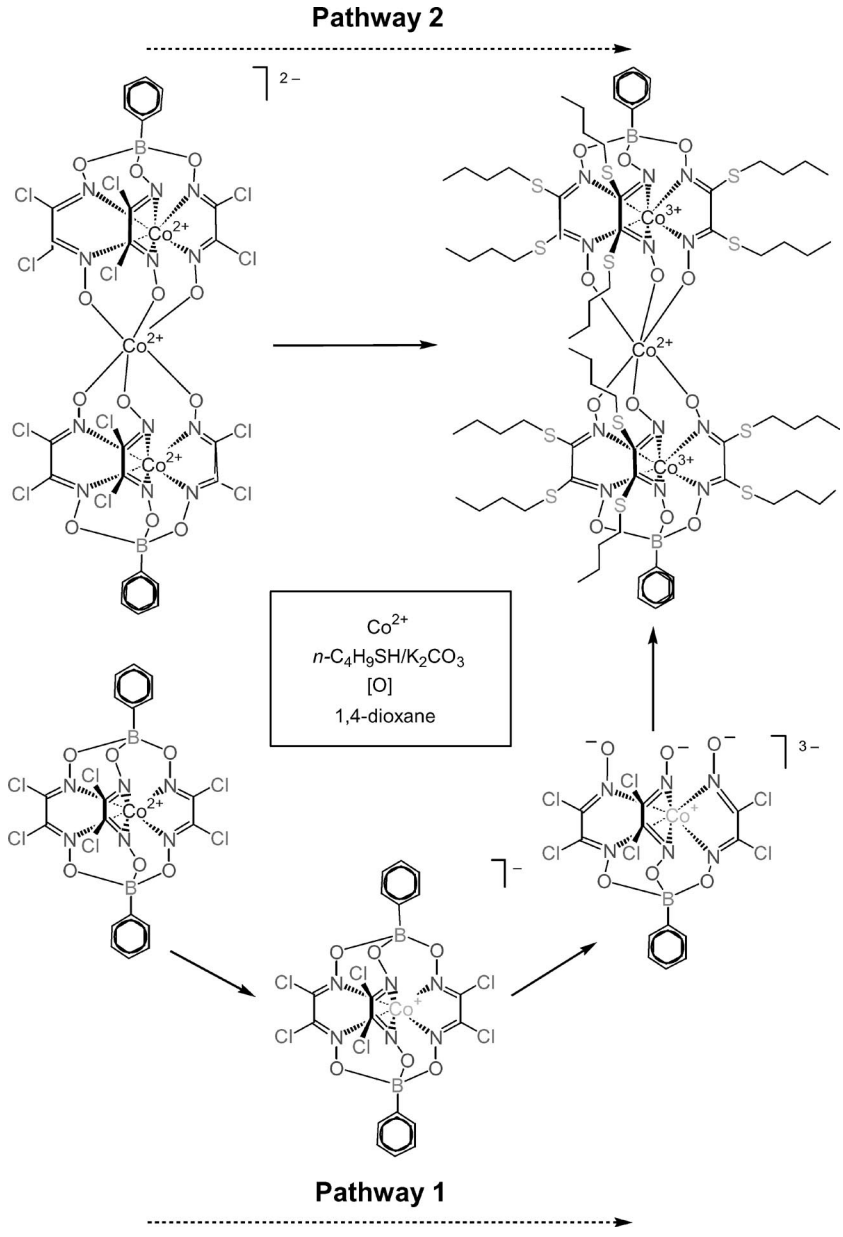

Scheme 2. Possible pathways to the trinuclear $Co^{III}Co^{II}Co^{III}$ bis-clathrochelate.

the dodecachlorine-containing bis-clathrochelate, which then undergoes a nucleophilic substitution and oxidation of the encapsulated cobalt ion. Finally, all these reactions (i.e., nucleophilic substitution, cross-linking, and oxidation of the encapsulated cobalt ion) may occur consecutively. It is also possible that the sample of $Co(Cl_2Gm)_3(BC_6H_5)_2$ used for functionalization contained an admixture of the dodecachlorine-containing bis-clathrochelate trinuclear Co^{II}-$Co^{II}Co^{II}$ complex (Scheme 2) because of the difficulties encountered in the purification of this phenylboron-capped precursor due to its low solubility. Functionalization of the dodecachlorine-containing complex in air could also lead to the dodeca-*n*-butylsulfide bis-clathrochelate. The formation of the halogen-containing bis-clathrochelate cobalt(III) precursor is hardly possible: we failed to implement both the chemical and electrochemical oxidations of an encapsulated cobalt(II) ion in the clathrochelate precursors without the destruction of the cage frameworks. We also failed to obtain and to isolate randomly the phenyl- and *n*-butylboron-capped dodecachlorine-containing cobalt(II) precursors. Thus, the first pathway (Scheme 2) to the trinuclear $Co^{III}Co^{II}Co^{III}$ bis-clathrochelate seems to be more probable.

We did, however, succeed in obtaining the hexachlorine-containing cobalt(I) clathrochelates: the reduction of brown solutions/suspensions of the cobalt(II) precursors in acetonitrile with metallic silver in the presence of tetraalkylammonium or tetra(dimethylamido)phosphonium halogenides (metallic silver forms an effective reducing system in the presence of halide ions when the concentration of its tetraalkylammonium or tetraamidophosphonium salts in acetonitrile is high) led to the formation of dark-blue solutions with the intensive coloration caused by the clathrochelate $[Co(Cl_2Gm)_3(BR)_2]^-$ anions. These anions were isolated as salts with bulky organic cations (Scheme 1), and the resulting navy blue solid products were air stable for several months but rapidly oxidized in solution. The relative stability of the cobalt(I) clathrochelates obtained accounts, to a great extent, for a strong electronic effect of six electron-withdrawing ribbed chlorine substituents in their α-dioximate fragments. In the case of the fluoroboron-capped cobalt(I) clathrochelate, the electron-withdrawing effect of the ribbed substituents increases at the expense of two fluorine apical atoms. Moreover, the oxidation of these solids with air oxygen is complicated by a dense packing of the organic cations and clathrochelate anions in crystals that prevents both the outer-sphere electron transfer from an encapsulated metal ion and the diffusion of oxygen molecules.

UV/Vis Spectra

The spectra of the cobalt(II) complexes synthesized, like those of their boron-capped aliphatic and aromatic tris-dioximate analogues,[1,2e] contain the intensive ($\varepsilon \approx 1–9 \times 10^3$ mol^{-1} L cm^{-1}) Md → Lπ* charge-transfer bands (CTBs) in the visible region: less intensive CTBs ($\varepsilon \approx 0.5–2 \times 10^3$ mol^{-1} L cm^{-1}) at 21230–24900 cm^{-1} were observed for the hexachlorine-containing precursors, and more intensive ($\varepsilon \approx 2–9 \times 10^3$ mol^{-1} L cm^{-1}) CTBs, which are considerably (by 1500–2000 cm^{-1}) longwave shifted, dominated in the spectra of the hexasulfide derivatives. The same effect was observed in the case of their iron and ruthenium(II)-containing analogues.[4,7]

The reduction of an encapsulated cobalt ion is responsible for the change in the color of the corresponding clathrochelate complexes from dark-brown to navy blue. The same blue color has been observed for the previously reported cobalt(I) complexes with nitrogen-containing ligands,[9] and it is determined by two highly intensive bands at approximately 15000 ($\varepsilon \approx 5–8 \times 10^3$ mol^{-1} L cm^{-1}) and 18500 ($\varepsilon \approx 4–7 \times 10^3$ mol^{-1} L cm^{-1}) cm^{-1}. These bands were assigned to the metal-to-ligand Md → Lπ* backdonation and ligand-to-metal Lπ → Md charge transfer.[9a,9b] It should be noted that, in the case of the cobalt tris-bipyridinates, the longwave shift of the CTB maximum upon going from the cobalt(II) ($\tilde{\nu}_{max} \approx 18180–18520$ cm^{-1}) to the cobalt(I) complex ($\tilde{\nu}_{max} \approx 16390–16670$ cm^{-1}) is only around 1800 cm^{-1}, whereas in the case of the obtained cobalt clathrochelates, the longwave shifts of the CTBs caused by the reduction of the encapsulated cobalt(II) ion to the cobalt(I) ion are from 5000 to 7000 cm^{-1}. Moreover, the intraligand π → π* transition bands in the UV region are shifted slightly to the shortwave region.

In the UV/Vis spectra of the synthesized hexaamine cobalt(III) clathrochelates, like in those of their aromatic and aliphatic clathrochelate analogues,[2e–2g] we found the bands of the d–d transitions $^1A_{1g} \rightarrow {}^1T_{1g}$ and $^1A_{1g} \rightarrow {}^1T_{2g}$ in the encapsulated Co^{3+} ion (see the Experimental Section and Table SI1 in the Supporting Information). As follows from this table, the field strengths of the clathrochelate amine ligands are substantially lower than those for their macrobicyclic analogues with aromatic and aliphatic substituents in chelate α-dioximate fragments.[2e–2g] This can be due to the considerable effect of six ribbed electron-donating alkylamine substituents with negative Hammett σ_{para} constants.

Magnetochemistry

Figure 1 shows the temperature dependence of the effective magnetic moments μ_{eff} of the hexachlorine-containing cobalt(II) clathrochelates with different apical substituents. The plot for the fluoroboron-capped clathrochelate $Co(Cl_2Gm)_3(BF)_2$ differs significantly from that of other cobalt(II) precursors: in its case, μ_{eff} (3.87 B.M. at 4 K) is close to the spin-only value for a high-spin molecule. This suggests that the high-spin state of the molecule $Co(Cl_2Gm)_3(BF)_2$ is preferably populated even at very low temperatures. Going from the fluoroboron-capped complex to its *n*-butylboron- and phenylboron-capped analogues, one can see the significant changes of the magnetochemical properties. The curves for the complexes $Co(Cl_2Gm)_3(Bn\text{-}C_4H_9)_2$ and $Co(Cl_2Gm)_3(BC_6H_5)_2$ (Figure 1) are characteristic of a gradual and incomplete spin doublet–quartet transition.[10]

At low temperatures, the μ_{eff} values (1.78 and 1.98 B.M., respectively) for both the *n*-butylboron- and phenylboron-capped cobalt(II) precursors are close to the characteristic value for systems with $s = ½$. The elevation of temperature led to a gradual increase in the μ_{eff} value. The transition temperature is lower for the phenylboron-capped complex than for its *n*-butylboron-containing analogue. At 300 K, the spin–spin transition is not complete for both the complexes; the population of the high-spin state is higher for the macrobicycle $Co(Cl_2Gm)_3(BC_6H_5)_2$ than for the clathrochelate $Co(Cl_2Gm)_3(Bn\text{-}C_4H_9)_2$ (based on spin-only values, the high-spin state populations are 0.8 and 0.5, respectively). In the case of the cobalt(II) complexes with less electron-withdrawing sulfide ribbed substituents, only the low-spin states are observed (Figure 2), and the values of μ_{eff} for the clathrochelates $Co\{(n\text{-}C_4H_9S)_2Gm\}_3(BC_6H_5)_2$ and $Co\{(C_6H_5S)_2Gm\}_3(Bn\text{-}C_4H_9)_2$ are in the range of 1.73–1.93 B.M. and do not change significantly with temperatures below 200 K. The μ_{eff} values for the complexes cobalt(I) $[(n\text{-}C_4H_9)_4N][Co^{I}(Cl_2Gm)_3(BF)_2]$ and $[(n\text{-}C_4H_9)_4N][Co^{I}(Cl_2Gm)_3(BC_6H_5)_2]$ (Figure 2) are temperature independent above 30 K and are characteristic of systems with $s = 1$ and $g = 2.0$ (the high-spin electronic configuration d^8).

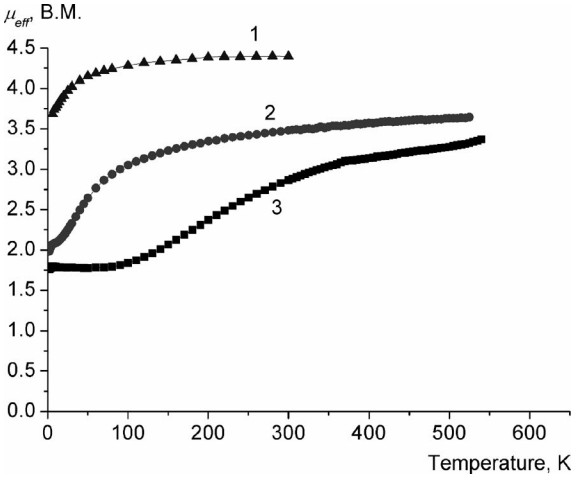

Figure 1. Temperature dependence of μ_{eff} for fine-crystalline samples $Co(Cl_2Gm)_3(BF)_2$ (▲, 1), $Co(Cl_2Gm)_3(BC_6H_5)_2$ (●, 2), and $Co(Cl_2Gm)_3(Bn\text{-}C_4H_9)_2$ (■, 3).

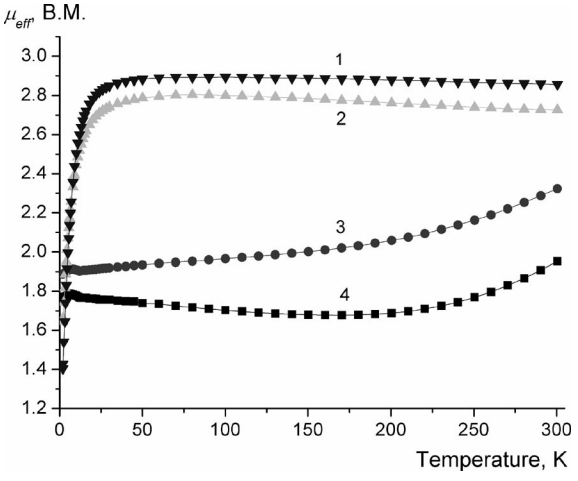

Figure 2. Temperature dependence of μ_{eff} for fine-crystalline samples $[(n\text{-}C_4H_9)_4N][Co(Cl_2Gm)_3(BC_6H_5)_2]$ (▼, 1), $[(n\text{-}C_4H_9)_4N][Co(Cl_2Gm)_3(BF)_2]$ (▲, 2), $Co\{(C_6H_5S)_2Gm\}_3(Bn\text{-}C_4H_9)_2$ (●, 3), and $Co\{(n\text{-}C_4H_9S)_2Gm\}_3(BC_6H_5)_2$ (■, 4).

NMR Spectra

The paramagnetic character of an encapsulated cobalt(II) ion complicated the interpretation of NMR spectra of the cobalt(II) clathrochelates obtained, and the 2D pulse sequences COSY and heteronuclear multiple quantum coherence (HMQC) were used to assign the signals in their ^1H and $^{13}C\{^1H\}$ NMR spectra (Table SI2 in the Supporting Information). The temperature-dependent paramagnetic shifts were observed in both the ^1H and the ^{13}C NMR spectra. Although Curie law holds for all these complexes, the different temperature dependence of the chemical shifts allowed us to separate them into two series with distinct magnetic properties. The ^1H NMR chemical shifts for the hexachlorine-containing cobalt(II) precursors are strongly temperature-dependent, whereas the spectra of the complexes $Co\{(C_6H_5S)_2Gm\}_3(Bn\text{-}C_4H_9)_2$ and $Co\{(n\text{-}C_4H_9S)_2Gm\}_3(BC_6H_5)_2$ change insignificantly with temperature. These data are in line with the conclusion that complexes $Co(Cl_2Gm)_3(Bn\text{-}C_4H_9)_2$ and $Co(Cl_2Gm)_3(BC_6H_5)_2$ are mostly in the high-spin state in solution at room temperature, whereas molecules $Co\{(C_6H_5S)_2Gm\}_3(Bn\text{-}C_4H_9)_2$ and $Co\{(n\text{-}C_4H_9S)_2Gm\}_3(BC_6H_5)_2$ are mostly in the low-spin state. This agrees well with the previously reported results, thus indicating the low-spin nature of cage cobalt(II) complexes with a strong-field macrobicyclic ligand.[2,11] The paramagnetic shift values also confirmed this tendency. In the ^1H NMR spectra of the hexachlorine-containing cobalt(II) clathrochelates, the signals of the protons of the apical groups are paramagnetically lowfield shifted compared to those for their diamagnetic iron(II)-containing analogues (Table SI2 in the Supporting Information). In the case of complex $Co(Cl_2Gm)_3(Bn\text{-}C_4H_9)_2$, the significant paramagnetic shift of the protons of the terminal methyl moieties, which are located at a distance of eight covalent bonds from the paramagnetic center, unambiguously proved the pseudocontact nature of these hyperfine shifts. In contrast, the signals of the protons of the *n*-butyl apical substituents in the spectrum of the complex $Co\{(C_6H_5S)_2Gm\}_3(Bn\text{-}C_4H_9)_2$ are hardly affected by the paramagnetic cobalt(II) ion. The only exception is the protons of the methylene groups of the capping O_3BCH_2 fragments; their signals are only slightly shifted to the highfield region as a result of the contact interaction. Similar trends were observed for the protons of the apical phenyl substituents of the clathrochelate $Co(Cl_2Gm)_3(BC_6H_5)_2$/$Co\{(n\text{-}C_4H_9S)_2Gm\}_3(BC_6H_5)_2$ pair. The dominance of the pseudocontact contribution to the paramagnetic shifts in the case of the complexes with the strong-field ligands, along with the insig-

nificant influence of the pseudocontact interaction on the NMR spectra of the complexes with the weak-field ligands, confirmed the preferential population of the high-spin state in the hexachlorine-containing cobalt(II) clathrochelates.

Complex $Co(Cl_2Gm)_3(BF)_2$ was not characterized by ^1H and ^{13}C NMR spectra: the signals of its azomethine carbon atoms were not observed in the spectra of the cobalt(II) complexes because of their paramagnetic broadening. The signal corresponding to the apical fluorine substituents in the ^{19}F NMR spectrum of this clathrochelate was found at δ = –60.7 ppm. The comparison of this value with those for the low-spin cobalt(II) complexes $CoDm_2Bd(BF)_2$ and $CoBd_2Dm(BF)_2$ (where Dm^{2-} and Bd^{2-} are dimethylglyoxime and α-benzyldioxime dianions, $\delta_{^{19}F}$ = –111.6 and –110.1 ppm, respectively[11]) and that for their diamagnetic iron(II) analogue[12] ($\delta_{^{19}F}$ = –90.5 ppm) demonstrated the opposite direction of the paramagnetic shift of the ^{19}F NMR signal for the complex $Co(Cl_2Gm)_3(BF)_2$. Such a dramatic change could occur only due to the preferential population of the high-spin state of this complex in solution at room temperature.

EPR Spectra

The glassy EPR spectra for most of the cobalt(II) clathrochelates obtained (Figure 3, Figures SI1–SI4 in the Supporting Information) are characteristic of the low-spin cobalt(II) complexes in the temperature range studied. These spectra demonstrate slightly rhombic *g* tensors (Table SI3) and contain the well-resolved eight-line splittings in the downfield region caused by the hyperfine interactions with ^{59}Co nucleus (I_{Co} = 7/2). In the case of the hexachlorine-containing precursors, the additional splittings result from interactions with donor nitrogen atoms. The five-line splitting pattern, which is clearly observed in the highfield region of the spectrum for the complex $Co(Cl_2Gm)_3(BF)_2$, suggests the interaction of an unpaired electron with only two nitrogen atoms. This may be caused by the Jahn–Teller distortion of the CoN_6-coordination polyhedron [i.e., the shift of the encapsulated cobalt(II) ion from its center] and therefore by nonequivalence of the nitrogen atoms.

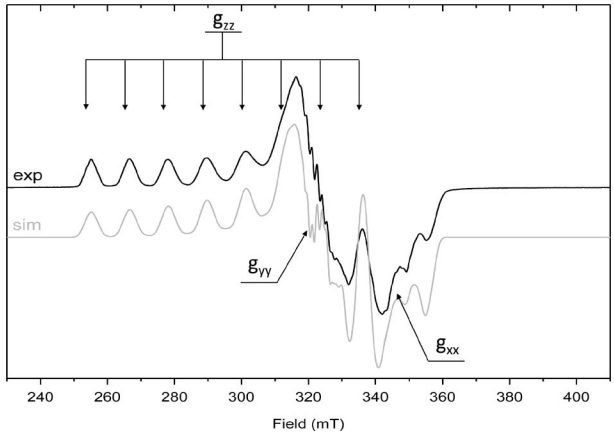

Figure 3. The glassy EPR spectrum of the solution of $Co(Cl_2Gm)_3(Bn\text{-}C_4H_9)_2$ in toluene at 30 K and the corresponding simulated spectrum.

Surprisingly, no EPR spectra characteristic of the high-spin cobalt(II) complexes were observed in the X-band in the temperature range studied. This could be explained in the case of the complex $Co(Cl_2Gm)_3(Bn\text{-}C_4H_9)_2$ as follows: the high-spin state becomes substantially populated only above 100 K, yet a very fast relaxation of the EPR signals of the high-spin cobalt(II) compounds makes it impossible to observe the spectra above 30 K.[13] According to the magnetometry data, however, the high-spin state should be significantly populated for the clathrochelate $Co(Cl_2Gm)_3(BC_6H_5)_2$, and especially for the complex $Co(Cl_2Gm)_3(BF)_2$ below 30 K. The absence of these signals may be caused by their considerable broadening because of the extremely fast relaxation that occurs even at low temperatures. For the complex $Co(Cl_2Gm)_3(BF)_2$ in solution, we were able to detect the signals of the low-spin Co^{2+} ion; this state is slightly populated even though the magnetometry data indicate the preferential high-spin state for this complex.

The population of the high-spin state in the powder sample $Co(Cl_2Gm)_3(BF)_2$ was confirmed by the temperature dependence of its EPR spectra at the Q-band (Figure SI5 in the Supporting Information). The lowfield broad signal is characteristic for the high-spin cobalt(II) complex with zero-field splitting larger than the microwave quantum.[13] Notably, it was possible to detect the signal at 150 K, even though its line width reaches approximately 600 mT, which prevented us from observing it at X-band. A decrease in the temperature leads to the narrowing of this line due to the slower relaxation at lower temperatures. At temperatures below 100 K, however, spin-crossover begins and this leads to the decrease and broadening of the signal of the high-spin cobalt(II) complex. The additional signal in the highfield region of the spectrum was assigned to the impurity (approximately 5%) of the decomposition product. The signal of the low-spin cobalt(II) clathrochelate expected in the same spectral region could not be reliably detected, probably due to the broadening caused by its exchange interaction with the remaining high-spin complex in the magnetically concentrated solid.

We attempted to register EPR spectra of the cobalt(I) clathrochelates $[(n\text{-}C_4H_9)_4N][Co^I(Cl_2Gm)_3(BF)_2]$ and $[(n\text{-}C_4H_9)_4N][Co^I(Cl_2Gm)_3(BC_6H_5)_2]$. According to the magnetometry data, these compounds are high-spin complexes with *s* = 1 at the temperatures above 30 K, but they were EPR silent in the X-band at all temperatures studied due to the long spin-lattice relaxation time as well as due to the magnitude and sign of the spin–orbital interaction and the ligand-field symmetry.[2i] Also, no EPR transitions were detected by EPR submillimeter spectroscopy in the range of 90–560 GHz at 4 K.[14]

In a nutshell, the EPR data are in good agreement with the magnetochemical results and showed that the low-spin state is populated at low temperatures in all the cobalt(II) complexes studied.

Structure of Complexes

The structural limitations of the clathrochelate ligand are caused by the cage framework (a macrobicyclic ligand without apical and ribbed substituents) rigidity governed by the energetics of its covalent bonds and bond angles.[2h] In the case of the boron-capped tris-dioximates, the macrobicyclic framework generally possesses D_3 symmetry with a threefold axis that passes through the capping boron atoms and three twofold axes that pass through the centers of C–C bonds in chelate dioximate fragments. The changes of torsion angles in B–O–N=C and N=C–C=N moieties allow a macrobicyclic cage to be distorted around the threefold B···B pseudoaxis. Other factors are caused by the interaction of an encapsulated metal ion with six donor nitrogen atoms of the three π-conjugated α-dioximate fragments of the clathrochelate ligand. Because the ribbed chelate cycles of a N_6-coordination polyhedron are formed by relatively rigid N=C–C=N fragments, the bite angle α (half of the chelate N–M–N angle, in which M is the corresponding encapsulated metal ion) remains practically the same, whereas the height h of this polyhedron varies with the distortion angle ϕ (Figure 4). On the one hand, a decrease in ϕ leads to an increase in h and permits one to encapsulate the relatively large metal ions (i.e., the Co^{2+}, Co^{+}, and Ru^{2+} cations). In particular, in the complexes $Co(Cl_2Gm)_3(Bn\text{-}C_4H_9)_2$, $Co(Cl_2Gm)_3(BF)_2$, $[(n\text{-}C_4H_9)_4N][Co(Cl_2Gm)_3(BC_6H_5)_2]$, and $\{[(CH_3)_2N]_4P\}[Co(Cl_2Gm)_3(Bn\text{-}C_4H_9)_2]$ with the encapsulated Co^{2+} and Co^{+} ions, the ϕ values are approximately 0° (see Tables SI4 and SI5 in the Supporting Information). On the other hand, in the case of the given encapsulated metal ion (therefore, with constant M–N distances), in going from small capping boron atoms to larger tin, germanium, and antimony cross-linking atoms, one can achieve a trigonal antiprismatic (TAP) geometry (ϕ = 60°),[1] which is optimal for the given electronic configuration of an encapsulated metal ion. Thus, these geometrical changes may be described as a rotational–translational elongation (shortening). In the case of the Co^{3+} and Fe^{2+} ions, when the size of a metal ion is smaller or close to the cavity size of a hypothetical free clathrochelate ligand, an increase in ϕ leads to a decrease in h. As a result, a macrobicyclic cage is able not only to adapt itself to an ion size, but also to utilize one more factor such as an energetic preference of a TAP geometry compared with a trigonal prismatic (TP) one (ϕ = 0°) for ions with electronic configurations d^6 (Fe^{2+}, Ru^{2+}, and Co^{3+}) and d^7 (Co^{2+}). The fine geometrical effects observed when going from one of these ions to other ions for labile polyamine macrobicyclic N_6-ligands have been described using the ligand-field stabilization energy (LFSE) concept.[2h]

With such a unique series of analogous complexes, in which an encapsulated cobalt ion has different oxidation [Co^{I}/Co^{II} and $Co^{II}/Co(III)$ pairs] and spin [½ ↔ ³/₂ for cobalt(II) ion] states, it was intriguing to analyze the relationship between the electronic configuration and spin state of this ion and the molecular geometry of its complexes. We also compared the structures of the cobalt, iron, and ruthenium(II) complexes (electronic configurations $3d^7$, $3d^6$, and $4d^6$, respectively) with the same tris-dichloroglyoximate clathrochelate ligand.

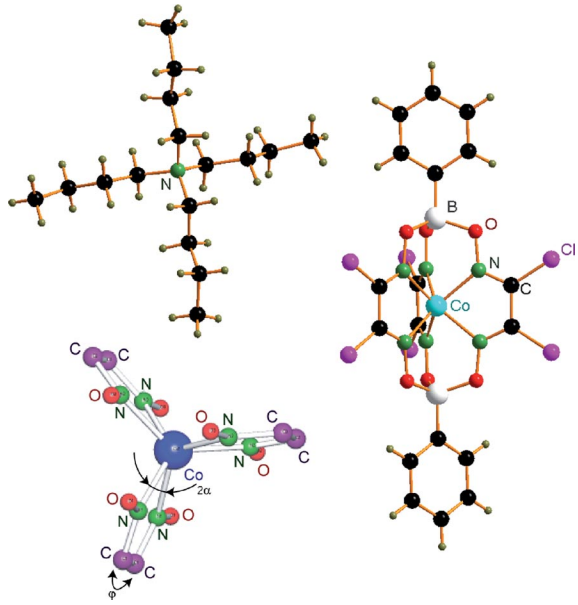

Figure 4. General view of the clathrochelate $[(n\text{-}C_4H_9)_4N][Co(Cl_2Gm)_3(BC_6H_5)_2]$ and its CoN_6-coordination polyhedron.

In the majority of the crystal structures studied, $Co(Cl_2Gm)_3(Bn\text{-}C_4H_9)_2$, $Co(Cl_2Gm)_3(BF)_2{\cdot}3C_6H_6$, $Co(Cl_2Gm)_3(BF)_2{\cdot}3C_6H_5CH_3$, $Co\{(n\text{-}C_4H_9S)_2Gm\}_3(BC_6H_5)_2$, an encapsulated cobalt ion is in the same oxidation state (2+) but the spin state is different. In the crystals of $Co(Cl_2Gm)_3(Bn\text{-}C_4H_9)_2$ and $Co\{(n\text{-}C_4H_9S)_2Gm\}_3(BC_6H_5)_2$ at 100 K, this ion is in the low-spin state with s = ½, as follows from the average Co–N distances (1.983 and 1.971 Å) and the significant variation of Co–N bond lengths (Table SI4 in the Supporting Information). The relatively wide range (ca. 0.16 Å) of the Co–N distances in the molecules $Co(Cl_2Gm)_3(Bn\text{-}C_4H_9)_2$ and $Co\{(n\text{-}C_4H_9S)_2Gm\}_3(BC_6H_5)_2$ resulted from a shift of an encapsulated metal ion in the direction of one of the three chelate dioximate fragments. The average Co–N distances for this fragment in both of these structures are 1.89 Å, whereas for two other chelate cycles the Co–N bond lengths are in the range of 2.04–2.05 Å. This fact may account for the Jahn–Teller distortion of the low-spin electronic configuration d^7 of a cobalt(II) ion. Furthermore, the observed geometry can be symmetry imposed for the cobalt ions in the molecules $Co(Cl_2Gm)_3(Bn\text{-}C_4H_9)_2$ and $Co\{(n\text{-}C_4H_9S)_2Gm\}_3(BC_6H_5)_2$, which are located on the C_2 symmetry axis.

To estimate the possible role of disorder in these two molecules, we analyzed the peculiarities of their thermal motion parameters. The anisotropic displacement parameters (ADPs)[15] may be used to estimate the ordering of the molecular species in a crystal. Even if there is no direct evidence of disorder, the ADP can be used to estimate the possible superposition of different tautomers, conformers, and so forth, thereby leading to the averaged geometry (see, for example, the ref.[16]). For ordered cobalt(II) complex in

the low-spin state, one can expect the long distances to be observed only for one of the three chelate fragments. Three equivalent structures can easily coexist in a crystal that would lead to their superposition and would reflect at least significant anisotropy of the thermal motion parameters of the cobalt ion. Indeed, the principal mean-square atomic displacements for the cobalt ion in the molecules $Co(Cl_2Gm)_3(Bn\text{-}C_4H_9)_2$ and $Co\{(n\text{-}C_4H_9S)_2Gm\}_3(BC_6H_5)_2$ at 100 K display significant anisotropy (Figure 5). In both these molecules, the maximal displacement was observed along the line perpendicular to the C_2 axis, and the "long" Co–N bonds correspond to the superposition of two Jahn–Teller distorted structures.

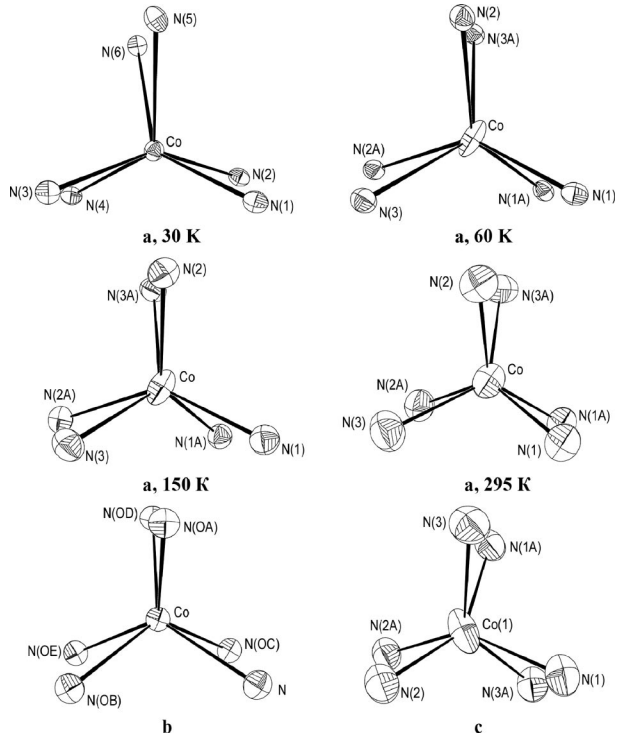

Figure 5. General views of the CoN_6-coordination polyhedra (atoms are represented by thermal ellipsoids) in the macrobicyclic complexes (a) $Co(Cl_2Gm)_3(Bn\text{-}C_4H_9)_2$ (at different temperatures), (b) $Co(Cl_2Gm)_3(BF)_2$, and (c) $Co\{(n\text{-}C_4H_9S)_2Gm\}_3(BC_6H_5)_2$. Thermal ellipsoids are drawn at the 50% probability level.

In contrast to clathrochelates $Co(Cl_2Gm)_3(Bn\text{-}C_4H_9)_2$ and $Co\{(n\text{-}C_4H_9S)_2Gm\}_3(BC_6H_5)_2$, in the complexes $Co(Cl_2Gm)_3(BF)_2\cdot 3C_6H_6$ and $Co(Cl_2Gm)_3(BF)_2\cdot 3C_6H_5CH_3$ at the same temperature, an encapsulated cobalt(II) ion is in the high-spin state with $s = 3/2$. In these isostructural crystals (space group $P6_3/m$) with the same clathrochelate cobalt(II) species and different solvent molecules (three benzene and three toluene ones, respectively), the cobalt ion is located in the center of an N_6-coordination polyhedron, and the Co–N distances are markedly longer [2.031(2)–2.033(2) Å] than those in the clathrochelates $Co(Cl_2Gm)_3(Bn\text{-}C_4H_9)_2$ and $Co\{(n\text{-}C_4H_9S)_2Gm\}_3(BC_6H_5)_2$. The difference between the average Co–N distances in complexes $Co(Cl_2Gm)_3(Bn\text{-}C_4H_9)_2$ and $Co\{(n\text{-}C_4H_9S)_2Gm\}_3(BC_6H_5)_2$ and that in $Co(Cl_2Gm)_3(BF)_2\cdot 3C_6H_6$ and $Co(Cl_2Gm)_3(BF)_2\cdot 3C_6H_5CH_3$ (ca. 0.05 Å) is slightly lower than the difference between the Shannon radii of the hexacoordinate high- and low-spin Co^{2+} ions (approximately 0.1 Å). No disorder was observed in the case of the fluoroboron-capped complexes (i.e., the thermal motion parameters of an encapsulated cobalt ion are almost isotropic). In their crystals, the aromatic solvate molecules, which surround the macrobicyclic species, are situated between the ribbed fragments that form the shortened contacts [3.347(2) Å] with the C–C bonds of the chelate N=C–C=N fragments (Figure 6). The distances between the π system of the macrobicyclic ligand and the solvate molecules are rather small, and they may be involved in stacking interactions. The latter should cause some charge redistribution in the ligand framework and may also affect the ϕ values. Apparently, this is an additional factor for the stabilization of TP geometry; these values for complexes $Co(Cl_2Gm)_3(BF)_2\cdot 3C_6H_6$ and $Co(Cl_2Gm)_3(Bn\text{-}C_4H_9)_2$ are equal to 0 and 7.8°, respectively. In contrast, the ϕ values in the diamagnetic hexachlorine-containing fluoroboron- and *n*-butylboron-capped iron(II) clathrochelates are almost identical (16.1 and 17.2°, respectively) (i.e., the apical substituents do not affect the geometry of the macrobicyclic frameworks).[4]

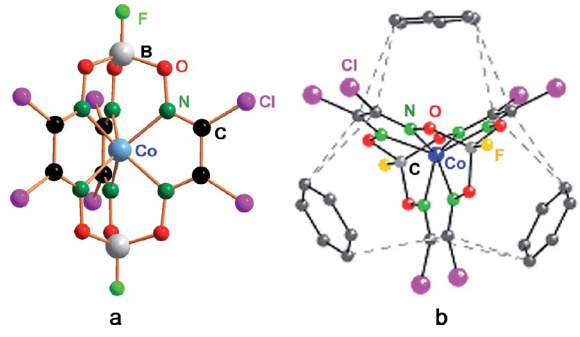

Figure 6. General views of the (a) macrobicyclic complex and (b) its solvate with benzene in crystal $Co(Cl_2Gm)_3(BF)_2\cdot 3C_6H_6$. Hydrogen atoms are omitted for clarity.

According to the magnetometry data, the spin state of an encapsulated cobalt(II) ion in molecule $Co(Cl_2Gm)_3(Bn\text{-}C_4H_9)_2$ is temperature dependent. Thus, we performed a multitemperature X-ray diffraction study of its single crystal in the temperature range of 30–295 K. Above 60 K, this ion demonstrates significant ADPs, and its maximal principal mean-square atomic displacement is almost constant (0.036–0.042 $Å^2$) in this temperature range (Table SI6 in the Supporting Information). The single crystal studied undergoes a structural phase transition at approximately 40–50 K from the base-centered cell (space group $C2/c$) to the primitive one ($P2_1/c$). This is in a good agreement with the previously described low-temperature calorimetric data.[17] The lowering of the site symmetry of a cobalt ion from C_2 to C_1 upon this phase transition in turn leads to the ordering of the crystal structure and causes changes of both the ADPs for the encapsulated ion and the variation of the Co–N distances. At 30 K, the principal mean square ADPs for this ion are equal to 0.008–0.010 $Å^2$, and the "long" distances were observed only for one of the three

chelate α-dioximate fragments [2.147(1)–2.095(1) Å], whereas other bonds of this type are markedly shorter [1.885(1)–1.901(1) Å]. The average Co–N distance is almost temperature independent and, thus can be used to estimate of the cobalt(II) ion spin state even in the case of disorder.

Both the ϕ value and the shift Δ of an encapsulated cobalt ion from the center of its N_6-coordination polyhedron decrease with temperature (Table SI7 in the Supporting Information). As the complex with the low-spin electronic configuration d^7 undergoes the Jahn–Teller distortion that causes an increase in these parameters, yet the high-spin state is almost distortionless, the X-ray diffraction data are in a good agreement with the magnetometry data. At low temperature, only the low-spin state of this cobalt(II) complex is populated, and the highest distortion of its coordination polyhedron is observed. The population of the high-spin state increases with temperature, and this causes a decrease in TAP distortion of the CoN_6 polyhedron. The linear regression, with $R = 0.99$ between Δ and μ_{eff}, is observed in the temperature range studied (Figure 7). If $\Delta = 0$ for the high-spin complex $Co(Cl_2Gm)_3(Bn\text{-}C_4H_9)_2$ and $\Delta = 0.11$ Å^2 for its low-spin state at $T = 60$ K, the populations of the doublet and quartet states may be calculated from this regression; almost all of the molecules $Co(Cl_2Gm)_3(Bn\text{-}C_4H_9)_2$ below 150 K are in the low-spin state.

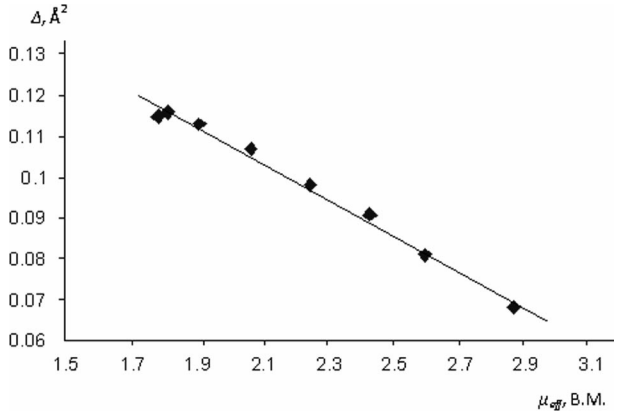

Figure 7. The plot of Δ versus μ_{eff} for $Co(Cl_2Gm)_2(Bn\text{-}C_4H_9)_2$ in the temperature range of 60–295 K.

The ordering of the crystal structure at 30 K means that only one Jahn–Teller distorted structure becomes the most energetically favorable. The discrimination of one of the three equivalent structures may be explained by the crystal packing effects. The crystal packing of complex $Co(Cl_2Gm)_3(Bn\text{-}C_4H_9)_2$ at 30 K (Figure 8) and above 60 K (Figure 9) is slightly different. From 30 to 60 K, each molecule forms two pairs of intermolecular contacts Cl(4)···O(4) and Cl(5)···O(5) with distances of approximately 3.20–3.23 Å and the angles C–Cl–O varying from 165 to 167°. As a result, the formation of the infinite supramolecular layers parallel to the (001) plane is observed (Figure 8). Both the "infinite layers" and the dimers are absent above 60 K; the phase transition may be caused by the additional contacts Cl···O formed at low temperatures.

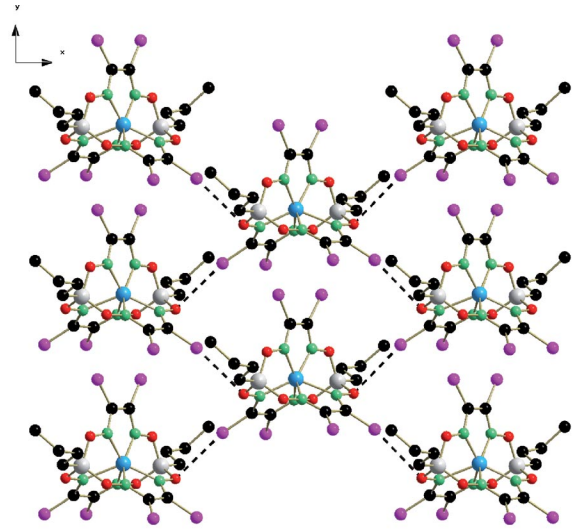

Figure 8. Packing diagram of $Co(Cl_2Gm)_3(Bn\text{-}C_4H_9)_2$ at 30 K.

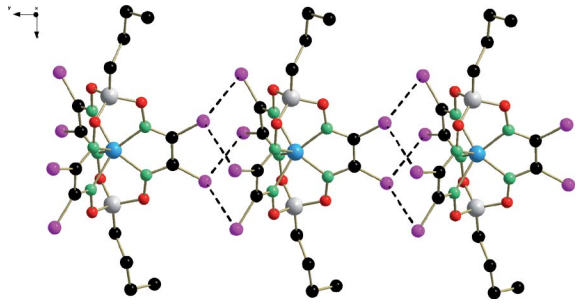

Figure 9. Packing diagram of $Co(Cl_2Gm)_3(Bn\text{-}C_4H_9)_2$ above 60 K.

Clathrochelate anions $[Co(Cl_2Gm)_3(Bn\text{-}C_4H_9)_2]^-$ crystallize with $\{[(CH_3)_2N]_4P\}^+$ cations and solvate benzene molecules; the crystal $[(n\text{-}C_4H_9)_4N][Co(Cl_2Gm)_3(BC_6H_5)_2]$ contains corresponding clathrochelate anions and $[(n\text{-}C_4H_9)_4N]^+$ cations (Figure 4). The Shannon radius of a cobalt(I) ion is assumed to be larger than that of the low-spin cobalt(II) ion, and, consequently, one could expect an increase in the average Co–N distance upon going from the cobalt(II) complex to the cobalt(I) clathrochelate with the same or the similar macrobicyclic ligand. In fact, this distance in complex $\{[(CH_3)_2N]_4P\}[Co(Cl_2Gm)_3(Bn\text{-}C_4H_9)_2]$ is approximately the same as in $[(n\text{-}C_4H_9)_4N][Co(Cl_2Gm)_3(BC_6H_5)_2]$ but exceeds that in $Co(Cl_2Gm)_3(Bn\text{-}C_4H_9)_2$ (Table SI4 in the Supporting Information). Nevertheless, the conclusion with regards to a systematic increase in the average Co–N distance upon going from the Co^{2+} ion to the Co^+ cation raises some doubts in this case because the ranges of the corresponding distances in the macrobicycles $Co(Cl_2Gm)_3(Bn\text{-}C_4H_9)_2$, $Co(Cl_2Gm)_3(BC_6H_5)_2$, $[Co(Cl_2Gm)_3(Bn\text{-}C_4H_9)_2]^-$, and $[Co(Cl_2Gm)_3(BC_6H_5)_2]^-$ significantly overlap.

The average B–O, N=C, =C–C=, and B–C distances in a macrobicyclic ligand are identical for all these complexes, and their values (Table SI4 in the Supporting Information) are close to tabular data.[18] A systematic increase in the average N–O and C–Cl distances from 1.354 to 1.367

(1.371) Å and from 1.698 to 1.716 (1.712) Å, respectively, was observed when going from cobalt(II) complex $Co(Cl_2Gm)_3(Bn\text{-}C_4H_9)_2$ to cobalt(I) clathrochelates $[(n\text{-}C_4H_9)_4N][Co(Cl_2Gm)_3(BC_6H_5)_2]$ and $\{[(CH_3)_2N]_4P\}[Co(Cl_2Gm)_3(Bn\text{-}C_4H_9)_2]$. Therefore, the average N=C–C=N torsion angle decreases from 4.0° in the molecule $Co(Cl_2Gm)_3(Bn\text{-}C_4H_9)_2$ to 3.1 and 1.0° for the complexes $[(n\text{-}C_4H_9)_4N][Co(Cl_2Gm)_3(BC_6H_5)_2]$ and $\{[(CH_3)_2N]_4P\}[Co(Cl_2Gm)_3(Bn\text{-}C_4H_9)_2]$ with a decrease in the TAP distortion of the coordination polyhedra: their macrobicyclic frameworks possess D_3 symmetry, which approaches D_{3h} in the latter cases. The main structural difference between the analogous cobalt(I) and cobalt(II) clathrochelates is a distortion around the C_3 axis: for the cobalt(II) N_6-coordination polyhedron $\phi = 7.8°$, whereas those of the encapsulated cobalt(I) ions are practically TP ($\phi = 1.3°$ for both the macrobicyclic anions $[Co(Cl_2Gm)_3(BC_6H_5)_2]^-$ and $[Co(Cl_2Gm)_3(Bn\text{-}C_4H_9)_2]^-$). The *h* values for these anions are higher than that for $Co(Cl_2Gm)_3(Bn\text{-}C_4H_9)_2$, but these changes (0.02 Å) are rather subtle. Thus, in this case, the variation of the coordination polyhedron geometry is described not only as its rotational–translational elongation (shortening) along the threefold axis, but also as its expansion (compression) along the twofold symmetry axes.

The capping cobalt(II) ion of the trinuclear $Co^{III}Co^{II}Co^{III}$ complex $\{[Co(n\text{-}C_4H_9S)_2Gm]_3(BC_6H_5)\}_2Co$ (Figure 10) is located in the inversion center. The encapsulated cobalt(III) ions and their nearest environments are, however, in the independent part of this molecule. The specific features of the ligand geometry in bis-clathrochelate $\{[Co(n\text{-}C_4H_9S)_2Gm]_3(BC_6H_5)\}_2Co$ result from the nonequivalence of its capping groups. The Co^{III}–N bond lengths in the molecule $\{[Co(n\text{-}C_4H_9S)_2Gm]_3(BC_6H_5)\}_2Co$ (Table SI5 in the Supporting Information) are shorter by 0.056 Å than the average Co^{II}–N distance (1.971 Å) in $Co[(n\text{-}C_4H_9S)_2Gm]_3(BC_6H_5)_2$ (Figure 11). This is in agreement with the increase in the Shannon radius of an encapsulated cobalt ion in the series: $lsCo^{3+} < lsCo^{2+} < hsCo^{2+}$. The coordination polyhedra of the encapsulated cobalt(III) ions in the bis-clathrochelate complex approaches a TAP ($\phi = 40.2°$), whereas the geometry of its monoclathrochelate cobalt(II)-containing analogue is close to a TP ($\phi = 14.5°$). As a result, the *h* value for the clathrochelate $\{[Co(n\text{-}C_4H_9S)_2Gm]_3(BC_6H_5)\}_2Co$ is smaller by 0.168 Å than that for $Co[(n\text{-}C_4H_9S)_2Gm]_3(BC_6H_5)_2$ (the average N···N distance in the coordination polyhedron bases is equal to 2.684 Å). The average N···N distances in the molecule $\{[Co(n\text{-}C_4H_9S)_2Gm]_3(BC_6H_5)\}_2Co$ are 2.617 and 2.737 Å for the boron- and cobalt(II)-adjacent TP bases, respectively. Thus, the coordination polyhedron of the cobalt(III) ion is a distorted truncated pyramid, and this ion is closer by 0.042 Å to its larger base.

In the series of the *n*-butylboron-capped tris-1,2-cyclohexanediondioximates,[2h] the following trends have been observed: the average M–N distances increase in the order Fe < Co < Ru, and the distortion angle ϕ increases as Co < Ru < Fe. In the series of the hexachlorine-containing clathrochelates, these relationships are as follows: Fe < Ru < Co and Ru < Co < Fe, respectively (Table SI4 in the Supporting Information). Thus, the same tendencies are observed for the iron and ruthenium(II) complexes with electronic configuration d^6. Other geometrical parameters, such as the N···N distances in the coordination polyhedron bases and the *h* value, demonstrate a similar trend in both series. The N···N distances change considerably in the orders Fe < Co = Ru and Fe < Co < Ru for 1,2-cyclohexanedioximate- and hexachlorine-containing macrobicyclic ligands, respectively. These distances have not been previously analyzed; however, in our opinion, they are an important characteristic of the interaction of an encapsulated metal ion with a macrobicyclic ligand.

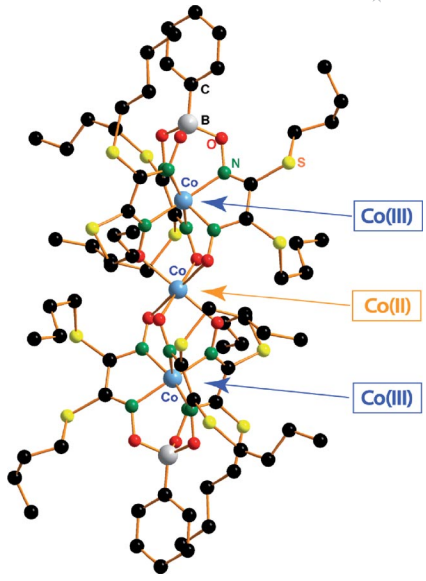

Figure 10. General view of the complex $Co^{III}Co^{II}Co^{III}\{Co[(n\text{-}C_4H_9S)_2Gm]_3(BC_6H_5)\}_2Co$. Hydrogen atoms are omitted for clarity.

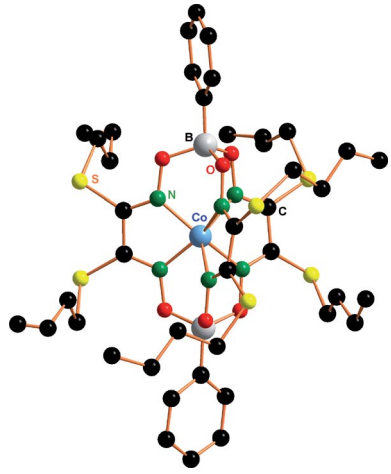

Figure 11. General view of the clathrochelate $Co[(n\text{-}C_4H_9S)_2Gm]_3(BC_6H_5)_2$. Hydrogen atoms are omitted for clarity.

Electrochemistry

The cyclic voltammograms (CVs) of the solutions of cobalt clathrochelates in dichloromethane with an ultra-

microelectrode as a working electrode demonstrate two waves with approximately equal diffusion-limit current in steady-state conditions. The cathodic wave corresponds to the Nernst one-electron process because its Tomeš criterion value is approximately 60 mV, and the wave slope, which was found from linearized function E versus $\ln[(i_d - i)/i]$, is close to RT/F. We assigned this process to the $Co^{+/2+}$ redox couple. It was additionally proven by the fact that the potentials of these waves coincided for both the preparatively obtained reduced and oxidized forms [i.e., the cobalt(I) and cobalt(II) clathrochelates with the same macrobicyclic ligands]. The anodic wave, assigned to the $Co^{2+/3+}$ redox couple, is quasireversible in the case of the chlorine-containing and sulfide clathrochelates, because it has a greater Tomeš criterion value. Such behavior was explained by specific interactions of these clathrochelates and/or the product of their oxidation with the material of an electrode. As a result, we failed to obtain CVs on an ultramicroelectrode for some clathrochelates (in particular, for the sulfide complexes). These interactions were not observed on the glassy carbon electrode, and two reversible one-electron oxidation events were registered (Figure 12). Their waves were slightly driven apart because of the ohmic drops in the low-conducting dichloromethane. The wave of the reference Fc/Fc^+ couple was also driven apart by the same value. In the case of an ultramicroelectrode, the signal of which is insensitive to the ohmic drops, the Nernst-type wave of the $Co^{+/2+}$ redox couple was observed.

Figure 12 and Table 1 show the influence of the substituents in α-dioximate chelate fragments on the redox potentials of an encapsulated cobalt ion. The electron-withdrawing ribbed substituents stabilize the lowest cobalt-ion oxidation state [i.e., that of cobalt(I)] because of electron-density delocalization over these substituents. As a result, both the clathrochelate cobalt(I) and cobalt(II) tris-dichloroglyoximates can be readily isolated preparatively, but we failed to obtain the corresponding cobalt(III) clathrochelates. The electron-donating substituents (in particular, alkylamine groups) stabilize the highest cobalt ion oxidation state, and in this case, only cobalt(III) complexes were synthesized. These results are in good agreement with the data on the macrobicyclic cobalt oximehydrazonates with electron-donating substituents in chelate fragments, for which both the cobalt(II) and cobalt(III) complexes were isolated preparatively.[19] The redox characteristics of both the $Co^{+/2+}$ and $Co^{2+/3+}$ couples for such complexes are very similar to those of the cobalt clathrochelates with electron-donating substituents.

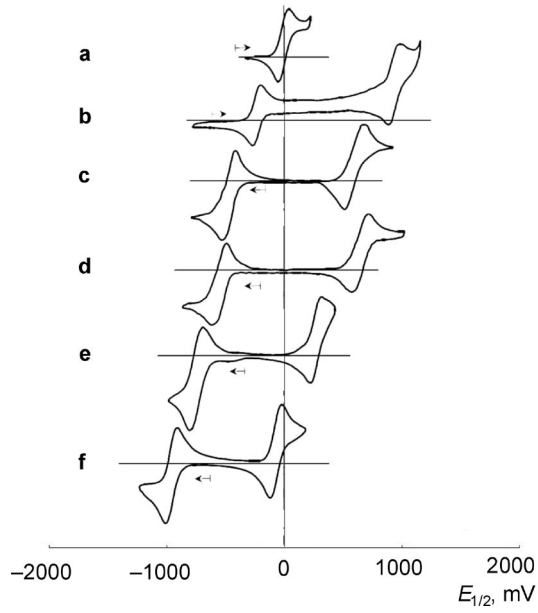

Figure 12. CVs of the cobalt clathrochelates obtained and those of ferrocene as an internal standard: (a) Fc; (b) $[(n\text{-}C_4H_9)_4N][Co(Cl_2Gm)_3(BF)_2]$; (c) $Co(Cl_2Gm)_3(Bn\text{-}C_4H_9)_2$; (d) $Co(Cl_2Gm)_3(BC_6H_5)_2$; (e) $Co\{(C_6H_5S)_2Gm\}_3(Bn\text{-}C_4H_9)_2$; (f) $Co\{(n\text{-}C_4H_9S)_2Gm\}_3(BC_6H_5)_2$.

Conclusion

As we have shown, the variation in ribbed substituents in a highly π-conjugated clathrochelate framework allows one to stabilize the target (highest or lowest) oxidation states of an encapsulated metal ion as well as to tune its spin state and redox characteristics. As a result, the compounds with previously unknown or unstable oxidation and spin states of an encapsulated metal ion might be synthesized, which is clearly of interest in both the theoretical and practical aspects.

Table 1. Cyclic voltammetric data [mV] for the obtained cobalt clathrochelates.[a]

Complex	Reduction $Co^{2+/+}$ redox couple			Oxidation $Co^{2+/3+}$ redox couple		
	$E_{1/2}$	ΔE_p	Current ratio[b]	$E_{1/2}$	ΔE_p	Current ratio[b]
$Co(Cl_2Gm)_3(BF)_2$	–270	90	0.85	970[c]		
$[Co(Cl_2Gm)_3(BC_6H_5)_2]^-$	–230	60	0.95	930	75	0.86
$Co(Cl_2Gm)_3(Bn\text{-}C_4H_9)_2$	–460	100	0.88	620	100	0.88
$[Co(Cl_2Gm)_3(Bn\text{-}C_4H_9)_2]^-$	–460	70	0.9	630	100	0.9
$Co(Cl_2Gm)_3(BC_6H_5)_2$	–500	90	1.16	690	90	0.99
$[Co(Cl_2Gm)_3(BC_6H_5)_2]^-$	–430	90	0.94	750	100	0.9
$Co\{(C_6H_5S)_2Gm\}_3(Bn\text{-}C_4H_9)_2$	–740	100	0.90	270	90	0.96
$Co\{(n\text{-}C_4H_9S)_2Gm\}_3(BC_6H_5)_2$	–960	80	0.95	–70	80	0.96

[a] Solvent: dichloromethane. A standard Ag/AgCl electrode was connected to the cell using a salt bridge. All potentials were referenced to the redox potential of the ferrocene Fc^+/Fc couple as an internal standard. [b] i^c_p/i^a_p for oxidation and i^c_p/i^a_p for reduction processes. [c] Oxidized form is insoluble and remains on the electrode. It reacts completely during the reverse scan. E^a_p reported.

Experimental Section

$Co(Cl_2Gm)_3(BC_6H_5)_2$: Dichloroglyoxime (Cl_2GmH_2, 5.5 g, 35 mmol) and phenylboronic acid (3.2 g, 25 mmol) were suspended/dissolved with stirring in dry boiling nitromethane (50 mL) under argon. Then solvent (20 mL) was distilled off to remove nitromethane–water azeotrope, and anhydrous $CoCl_2$ (1.3 g, 10 mmol) was added. The reaction mixture was heated at reflux with stirring for 10 h and filtered off. The dark-brown precipitate was washed with hot methanol, diethyl ether, hexane, and dried in vacuo; yield 5.5 g (71%). $C_{18}H_{10}B_2Cl_6CoN_6O_6$ (699.59): calcd. C 30.88, H 1.43, N 12.01, Co 8.42, Cl 30.45; found C 30.90, H 1.45, N 11.94, Co 8.36, Cl 30.44. MS (PD): *m*/*z* (%) = 700 (30) $[M]^+$, 578 (100) $[M - Cl_2C_2N_2]^{+\cdot}$. UV/Vis ($CHCl_3$): $\tilde{\nu}_{max}$ (10^{-3} ε, $mol^{-1}\,L\,cm^{-1}$) = 21230 (2.2), 23360 (1.0), 27400 (3.1), 31150 (3.9), 33670(4.6), 37600 (24) cm^{-1}. IR (KBr): $\tilde{\nu}$ = 1567 [ν(C=N)], 892–910 (m), 963–976 (m), 1086 [ν(N–O)] , 1228 [m, ν(B–O)] cm^{-1}.

$Co(Cl_2Gm)_3(Bn\text{-}C_4H_9)_2$: Cl_2GmH_2 (5.5 g, 35 mmol) and *n*-butylboronic acid (2.6 g, 26 mmol) were dissolved/suspended with stirring in dry boiling nitromethane (50 mL) under argon. Then solvent (20 mL) was distilled off, and anhydrous $CoCl_2$ (1.3 g, 10 mmol) was added. The reaction mixture was heated at reflux with intensive stirring for 8 h and cooled to room temperature. The microcrystalline dark-brown product was filtered, dried in vacuo, and dissolved in dichloromethane. The solution obtained was filtered through a silica gel Silasorb SPH-300 (30 mm layer), evaporated to a small volume, and precipitated with a threefold volume of hexane. The precipitate obtained was filtered, washed with hexane, and dried in vacuo; yield 1.7 g (26%). $C_{14}H_{18}B_2Cl_6CoN_6O_6$ (659.61): calcd. C 25.47, H 2.73, N 12.74, Co 8.93; found C 25.42, H 2.74, N 12.73, Co 8.81. MS (PD): *m*/*z* (%) = 660 (75) $[M]^{+\cdot}$, 538 (100) $[M - Cl_2C_2N_2]^{+\cdot}$. UV/Vis (THF): $\tilde{\nu}_{max}$ (10^{-3} ε, $mol^{-1}\,L\,cm^{-1}$) = 21370 (1.6), 23750 (0.64), 27170 (3.2), 30400 (3.1), 34840 (8.4), 37450 (20) cm^{-1}. IR (KBr): $\tilde{\nu}$ = 1562 [ν(C=N)] , 895 (m), 938 (m), 1052 [ν(N–O)], 1101 [m, ν(B–O)] cm^{-1}.

$Co(Cl_2Gm)_3(BF)_2$: Cl_2GmH_2 (4.7 g, 30 mmol), fine pulverized anhydrous $CoCl_2$ (1.3 g, 10 mmol), and $(BOF)_3$ (1.84 g, 40 mmol) were suspended/dissolved with stirring in nitromethane (30 mL) under argon. The light-blue reaction mixture was stirred at 125 °C for 10 min with partial distillation of a solvent (15 mL), and the freshly distilled $BF_3{\cdot}O(C_2H_5)_2$ (5 mL, 40 mmol) was added dropwise to the boiling mixture. Then nitromethane (20 mL) was added, and the reaction mixture was heated at 125–130 °C for 30 min, and $BF_3{\cdot}O(C_2H_5)_2$ (5 mL, 40 mmol) and dichloroglyoxime (1.57 g, 10 mmol) were added. The dark-brown reaction mixture was heated at the same temperature with partial distillation of a solvent for 40 min (the final volume of the reaction mixture was 20 mL). The reaction mixture was left overnight, and dichloromethane (50 mL) was added. The solution obtained was washed with water, dried with $CaCl_2$, filtered through a silica gel Silasorb SPH-300 (30 mm layer), and the solvents evaporated to dryness. The solid residue was dissolved in chloroform (30 mL). The chloroform solution was filtered through a silica gel Silasorb SPH-300 (30 mm layer), and then heptane (40 mL) was added. The filtrate was rotary evaporated to $^1/_3$ volume, the dark-brown precipitate formed was filtered, washed with heptane, and dried in vacuo; yield 1.8 g (31%). $C_{60}B_2Cl_6CoF_2N_6O_6$ (583.37): calcd. C 12.34, N 14.40, Co 10.09, Cl 36.50; found C 12.54, N 14.30, Co 10.08, Cl 36.38. MS (PD): *m*/*z* (%) = 584 (60) $[M]^{+\cdot}$, 462 (100) $[M - Cl_2C_2N_2]^{+\cdot}$. UV/Vis (THF): $\tilde{\nu}_{max}$ (10^{-3} ε, $mol^{-1}\,L\,cm^{-1}$) = 21930 (0.75), 24900 (0.53), 27250 (1.9), 29330 (2.4), 35330 (7.0), 38170 (16) cm^{-1}. IR (KBr): $\tilde{\nu}$ = 1572 [ν(C=N)], 923–940 (m), 1101 [ν(N–O)], 1223 [m, ν(B–O) + ν(B–F)] cm^{-1}.

$[(n\text{-}C_4H_9)_4N][Co(Cl_2Gm)_3(BC_6H_5)_2]$: Complex $Co(Cl_2Gm)_3(BC_6H_5)_2$ (0.31 g, 0.44 mmol), silver powder (0.24 g, 2.2 mmol) and $[(n\text{-}C_4H_9)_4N]I$ (0.16 g, 0.44 mmol) were dissolved/suspended in acetonitrile/dichloromethane (3:1) mixture (10 mL) under argon. The reaction mixture was stirred for 2 h and then evaporated in vacuo to dryness. The dark-blue solid was washed with methanol (3 mL), benzene/hexane (1:1) mixture (10 mL), and dissolved in dichloromethane. The solution was filtered under argon and precipitated with hexane. The product was washed with hexane and dried in vacuo; yield 0.39 g (94%). $C_{34}H_{46}B_2Cl_6CoN_7O_6$ (942.06): calcd. C 43.34, H 4.89, N 10.41, Co 6.26; found C 43.23, H 4.80, N 10.41, Co 6.12. MS (PD): *m*/*z* (positive range) = 917 $[M - Cl^-]^+$; *m*/*z* (%) (negative range) = –700 (100) $[M - (n\text{-}C_4H_9)_4N^+]^-$, –681 (40) $[M - (n\text{-}C_4H_9)_4N^+ - F]^-$. UV/Vis ($CH_3CN$): $\tilde{\nu}_{max}$ (10^{-3} ε, $mol^{-1}\,L\,cm^{-1}$) = 14700 (5.3), 18400 (4.5), 21980 (0.8), 24100 (0.8), 26530 (2.1), 34600 (4.8), 39530 (21) cm^{-1}. IR (KBr): $\tilde{\nu}$ = 1512 [ν(C=N)], 886–898 (m), 956, 1008 [ν(N–O)], 1218 [m, ν(B–O)] cm^{-1}.

$\{[(CH_3)_2N]_4P\}[Co(Cl_2Gm)_3(Bn\text{-}C_4H_9)_2]$: Complex $Co(Cl_2Gm)_3(Bn\text{-}C_4H_9)_2$ (0.66 g, 1 mmol), an excess amount of silver powder (0.44 g, 4.1 mmol), potassium iodide (0.18 g, 1.1 mmol), and $\{[(CH_3)_2N]_4P\}BF_4$ (0.30 g, 1.06 mmol) were dissolved/suspended in a dichloromethane/methanol (2:1) mixture (20 mL) under argon. The reaction mixture was stirred for 8 h, and then the dark-blue solution/suspension formed was evaporated with stirring in vacuo to dryness. The solid residue was dissolved in a benzene/dichloromethane (6:1) mixture, filtered, and evaporated to half volume. Then the product was precipitated with hexane, washed with hexane, and dried in vacuo; yield 0.67 g (77%). $C_{22}H_{42}B_2Cl_6CoN_{10}O_6P$ (866.89): calcd. C 43.34, H 4.89, N 10.41, Co 6.26; found C 43.23, H 4.80, N 10.41, Co 6.12. MS (PD): *m*/*z* (positive range) = 917 $[M - Cl^-]^{+\cdot}$; *m*/*z* (negative range) = –660 $[M - ((CH_3)_2N)_4P^+]^-$. UV/Vis (CH_3CN): $\tilde{\nu}_{max}$ (10^{-3} ε, $mol^{-1}\,L\,cm^{-1}$) = 14700 (8.0), 18380 (6.6), 22420 (0.6), 24330 (0.5), 26600 (2.6), 31250 (2.4), 39680 (22) cm^{-1}. IR (KBr): $\tilde{\nu}$ = 1512 [ν(C=N)], 846, 909, 956, 997 (m), 1008 [ν(N–O)], 1094 [m, ν(B–O)] cm^{-1}.

$[(n\text{-}C_4H_9)_4N][Co(Cl_2Gm)_3(BF)_2]$: Complex $Co(Cl_2Gm)_3(BF)_2$ (0.25 g, 0.43 mmol), $[(n\text{-}C_4H_9)_4N]I$ (0.17 g, 0.46 mmol), and an excess amount of silver powder (0.30 g, 2.8 mmol) were dissolved/suspended in an acetonitrile/benzene (20:1) mixture (10.5 mL) under argon. The reaction mixture was stirred for 30 min, and the dark-blue solution/suspension formed was evaporated with stirring in vacuo to dryness. The solid residue was washed with methanol (6 mL, in two portions), a small amount of benzene, hexane, and dried in vacuo; yield 0.31 g (88%). $C_{22}H_{36}N_7O_6B_2CoCl_6F_2$ (825.84): calcd. C 31.98, H 4.36, N 11.63, Co 7.14; found C 31.71, H 4.35, N 11.52, Co 7.01. MS (PD): *m*/*z* (positive range) = 1068 $[M + (n\text{-}C_4H_9)_4N^+]^+$; *m*/*z* (%) (negative range) = –584 (100) $[M - (n\text{-}C_4H_9)_4N^+]^-$, –565 (20) $[M - (n\text{-}C_4H_9)_4N^+ - F]^-$. UV/Vis ($CH_3CN$): $\tilde{\nu}_{max}$ (10^{-3} ε, $mol^{-1}\,L\,cm^{-1}$) = 14810 (5.7), 18480 (4.7), 22080 (0.7), 23530 (0.6), 26740 (2.4), 35090 (3.6), 40650 (15) cm^{-1}. IR (KBr): $\tilde{\nu}$ = 1525 [ν(C=N)], 923 (m), 1030 [ν(N–O)], 1186 [ν(B–O) + ν(B–F)] cm^{-1}.

$Co\{(n\text{-}C_4H_9S)_2Gm\}_3(BC_6H_5)_2$: Complex $Co(Cl_2Gm)_3(BC_6H_5)_2$ (0.70 g, 1 mmol) and an excess of $n\text{-}C_4H_9SH$ (0.7 mL, 7 mmol) were dissolved/suspended in dichloromethane (10 mL). A solution of triethylamine (1 mL, 7 mmol) in dichloromethane (5 mL) was added dropwise to the stirring reaction mixture for 3 h, and the resulting dark-brown solution was washed with Na_2CO_3 saturated aqueous solution (100 ml; in two portions) and water (100 mL, in two portions). The dichloromethane extract was dried with $MgSO_4$ and the solvents evaporated to dryness. The solid residue was washed with methanol, a small amount of hexane and dissolved in

a dichloromethane/hexane (1:10) mixture. The solution was filtered through a silica gel Silasorb SPH-300 (30 mm layer) and slowly evaporated to dryness. The dark-brown crystals were washed with hexane and dried in vacuo; yield 0.68 g (67%). $C_{42}H_{64}N_6O_6B_2CoS_6$ (1021.96): calcd. C 49.31, H 6.26, N 8.22, Co 5.76; found C 49.32, H 6.15, N 8.22, Co, 5.66. MS (PD): *m*/*z* = 1022 $[M]^{+\cdot}$. UV/Vis (CH_2Cl_2): $\tilde{\nu}_{max}$ (10^{-3} ε $mol^{-1}\,L\,cm^{-1}$) = 19380 (5.7), 21140 (2.2), 24880 (6.8), 31850 (11), 42200 (31) cm^{-1}. IR (KBr): $\tilde{\nu}$ = 1590 [ν(C=N)] , 890, 933, 972 [ν(N–O)], 1222 [m, ν(B–O)] cm^{-1}.

Co{$(C_6H_5S)_2Gm$}$_3$(Bn-C_4H_9)$_2$: This complex was synthesized like the previous one except that complex $Co(Cl_2Gm)_3(Bn\text{-}C_4H_9)_2$ (0.66 g, 1 mmol) and thiophenol (0.7 mL, 7 mmol) were used instead of $[Co(Cl_2Gm)_3(BC_6H_5)_2]$ and n-C_4H_9SH; yield 0.57 g (52%). $C_{50}H_{48}N_6O_6B_2CoS_6$ (1101.92): calcd. C, 54.50; H, 4.36; N, 7.63; Co, 5.35; found C, 54.54; H, 4.31; N, 7.72; Co, 5.38%. MS (PD): *m*/*z* = 1101 $[M]^{+\cdot}$. UV/Vis (CH_2Cl_2): $\tilde{\nu}_{max}$ (10^{-3} ε, $mol^{-1}\,L\,cm^{-1}$) = 19920 (9.5), 25380 (11), 30500 (6.9) cm^{-1}. IR (KBr): $\tilde{\nu}$ = 1580 [ν(C=N)], 932 (m), 1043 [m, ν(N–O)], 1098 [m, ν(B–O)] cm^{-1}.

[Co{(n-$C_4H_9NH)_2Gm$}$_3$(BC_6H_5)$_2$](ClO$_4$): Complex $Co(Cl_2Gm)_3(BC_6H_5)_2$ (0.70 g, 1 mmol) was dissolved/suspended in dry DMF (10 mL), and a solution of n-butylamine (1.8 mL, 18 mmol) in DMF (10 mL) was added dropwise to the stirred reaction mixture for 2 h under argon. The reaction mixture was left overnight and then was stirred for 10 h in air. The red-brown solution was precipitated with water (40 mL). The product was filtered, re-precipitated from DMF with $NaClO_4$ saturated aqueous solution, washed with methanol/water (1:1) mixture, and dried. The solid was dissolved in dichloromethane, and the extract was filtered through a silica gel Silasorb SPH-300 (30 mm layer). The dichloromethane elute was thrown out, and the product was eluted with dichloromethane/acetonitrile 20:1 mixture. The red-brown elute was evaporated to dryness, the solid residue was re-precipitated from chloroform with hexane, washed with diethyl ether, hexane, and dried in vacuo; yield 0.53 g (52%). $C_{42}H_{70}N_{12}O_{10}B_2CoCl$ (1019.10): calcd. C 49.51, H 6.88, N 16.50, Co 5.79; found C 49.39, H 6.89, N 16.28, Co 5.83. MS (PD): *m*/*z* = 919 $[M - ClO_4^-]^+$. ^{1}H NMR ($CDCl_3$): δ = 0.85 (t, 18 H, CH_3), 1.31 (m, 12 H, CH_2), 1.63 (m, 12 H, CH_2), 3.69 (m, 12 H, NCH_2), 6.27 (m, 6 H, NH), 7.34 (m, 6 H, Ph), 7.59 (m, 4 H, Ph) ppm. $^{13}C\{^1H\}$ NMR ($CDCl_3$): δ = 13.5 (s, CH_3), 19.4 (s, CH_2), 33.3 (s, CH_2), 45.4 (s, NCH_2), 127.2 (s, Ph), 127.6 (s, Ph), 131.1 (s, Ph), 140.9 (br. s, C–B), 151.9 (s, C=N) ppm. UV/Vis ($CHCl_3$): $\tilde{\nu}_{max}$ (10^{-3} ε, $mol^{-1}\,L\,cm^{-1}$) = 17000 (0.58), 19600 (1.5), 23870 (1.6), 26670 (4.7), 29850 (10), 36100 (27) cm^{-1}. IR (KBr): $\tilde{\nu}$ = 1610 [m, ν(C=N) + δ(N–H)] , 878, 932, 956, 1054, 1099 [m, ν(N–O)], 1218 [m, ν(B–O)] cm^{-1}.

[Co{(n-$C_4H_9NH)_2Gm$}$_3$(BF)$_2$](ClO$_4$): This complex was synthesized like the previous one except that $Co(Cl_2Gm)_3(BF)_2$ (0.58 g, 1 mmol) was used instead of $Co(Cl_2Gm)_3(BC_6H_5)_2$; yield 0.32 g (35%). $C_{30}H_{60}N_{12}O_{10}B_2CoClF_2$ (902.87): calcd. C 39.91, H 6.65, N 18.63, Co 6.53; found C 40.01, H 6.78, N 18.65, Co 6.56. MS (PD): *m*/*z* = 802 $[M - ClO_4^-]^+$. ^{1}H NMR ($CDCl_3$): δ = 0.87 (t, 18 H, CH_3), 1.34 (m, 12 H, CH_2), 1.61 (m, 12 H, CH_2), 3.63 (m, 12 H, NCH_2), 6.62 (m, 6 H, NH) ppm. $^{13}C\{^1H\}$ NMR ($CDCl_3$): δ = 13.5 (s, CH_3), 19.4 (s, CH_2), 33.1 (s, CH_2), 45.3 (s, NCH_2), 151.8 (s, C=N) ppm. UV/Vis ($CHCl_3$): $\tilde{\nu}_{max}$ (10^{-3} ε, $mol^{-1}\,L\,cm^{-1}$) = 16700 (0.25), 18730 (1.2), 25300 (2.5), 28400 (4.1), 31060 (7.8), 35000 (6.5), 39220 (21) cm^{-1}. IR (KBr): $\tilde{\nu}$ = 1622 [m, δ(N–H) + ν(C=N)] , 888 (m), 930, 941, 1061, 1100 [ν(N–O) , 1155–1180 [m, ν(B–O) + ν(B–F)] , 1218 [m, ν(B–O)] cm^{-1}.

[Co{($tert$-$C_4H_9NH)_2Gm$}$_3$(BC_6H_5)$_2$](ClO$_4$): This complex was synthesized like the clathrochelate $[Co\{(n\text{-}C_4H_9NH)_2Gm\}_3(BC_6H_5)_2](ClO_4)$ except that $tert$-butylamine (1.9 mL, 18 mmol) was used instead of n-butylamine; yield 0.33 g (32%). $C_{42}H_{70}N_{12}O_{10}B_2CoCl$ (1019.10): calcd. C 49.51, H 6.88, N 16.50, Co 5.79; found C 49.41, H 6.84, N 16.56, Co 5.61. MS (PD): *m*/*z* = 919 $[M - ClO_4^-]^+$. ^{1}H NMR ($CDCl_3$): δ = 1.47 (c, 54 H, CH_3), 5.82 (c, 6 H, NH), 7.31 (m, 6 H, Ph), 7.71 (m, 4 H, Ph) ppm. $^{13}C\{^1H\}$ NMR ($CDCl_3$): δ = 31.3 (s, CH_3), 57.3 [s, $C(CH_3)_3$], 127.0 (s, Ph), 127.6 (s, Ph), 131.9 (s, Ph), 152.8 (s, C=N) ppm. UV/Vis ($CHCl_3$): $\tilde{\nu}_{max}$ (10^{-3} ε, $mol^{-1}\,L\,cm^{-1}$) = 16840 (0.53), 19960 (1.1), 29590 (2.0), 29760 (9.2), 36360 (24) cm^{-1}. IR (KBr): $\tilde{\nu}$ = 1598, 1640 [ν(C=N) + δ(N–H) , 895 (m), 945, 1030–1035 (m), 1087 [ν(N–O)], 1213 [m, ν(B–O)] cm^{-1}.

[Co{($C_6H_{11}NH)_2Gm$}$_3$(BC_6H_5)$_2$](ClO$_4$): This complex was synthesized like the clathrochelate $[Co\{(n\text{-}C_4H_9NH)_2Gm\}_3(BC_6H_5)_2](ClO_4)$ except that cyclohexylamine (2.1 mL, 18 mmol) was used instead of n-butylamine; yield 0.55 g (47%). $C_{54}H_{82}N_{12}O_{10}B_2CoCl$ (1175.33): calcd. C 55.20, H 6.98, N 14.31, Co 5.02; found C 55.17, H 6.97, N 14.14, Co 4.94. MS (PD): *m*/*z* = 1075 $[M - ClO_4^-]^+$. ^{1}H NMR ($CDCl_3$): δ = 1.29–1.68 [m, 48 H, (α + β + γ)–CH_2], 2.02 (m, 12 H, α′–CH_2), 4.21 (m, 6 H, CH), 6.37 (m, 6 H, NH), 7.35 (m, 6 H, Ph), 7.64 (m, 4 H, Ph) ppm. $^{13}C\{^1H\}$ NMR ($CDCl_3$): δ = 24.8 [s, (β + γ)–CH_2], 33.5 (s, α–CH_2), 34.6 (s, α′–CH_2), 54.8 (s, CH), 127.0 (s, Ph), 127.4 (s, Ph), 131.2 (s, Ph), 151.3 (s, C=N) ppm. UV/Vis ($CHCl_3$): $\tilde{\nu}_{max}$ (10^{-3} ε, $mol^{-1}\,L\,cm^{-1}$) = 17540 (0.67), 20080 (1.5), 26670 (3.5), 28570 (6.0), 30300 (5.4), 36100 (28) cm^{-1}. IR (KBr): $\tilde{\nu}$ = 1582 [m, ν(C=N) + δ(N–H)] , 896 (m), 944, 1049, 1075 [ν(N–O)], 1217 [m, ν(B–O)] cm^{-1}.

{Co[(n-$C_4H_9S)_2Gm$]$_3$(BC_6H_5)}$_2$Co: Single crystals of this complex were obtained by slow evaporation of the hexane extract from the synthesis of the clathrochelate $Co\{(n\text{-}C_4H_9S)_2Gm\}_3(BC_6H_5)_2$ in 1,4-dioxane with the n-C_4H_9SH/K_2CO_3 system as a thiolate anion source. MS (MALDI-TOF): *m*/*z* = 1950 $[M + Na^+]^+$, 1928 $[M + H^+]^+$, 1862 $[M - n\text{-}C_4H_9S + Na^+]^+$, 1840 $[M - n\text{-}C_4H_9S + H^+]^+$. UV/Vis ($CHCl_3$): $\tilde{\nu}_{max}$ = 21280, 22120, 25250, 28490, 32900, 39220 cm^{-1}.

X-ray Crystallography: The details of crystal data collection and refinement for complexes $Co(Cl_2Gm)_3(Bn\text{-}C_4H_9)_2$, $Co(Cl_2Gm)_3(BF)_2{\cdot}3C_6H_6$, $Co(Cl_2Gm)_3(BF)_2{\cdot}3C_6H_5CH_3$, $[(n\text{-}C_4H_9)_4N][Co(Cl_2Gm)_3(BC_6H_5)_2]$, $Co\{(n\text{-}C_4H_9S)_2Gm\}_3(BC_6H_5)_2$, and $\{Co[(n\text{-}C_4H_9S)_2Gm]_3(BC_6H_5)\}_2Co$ are listed in Table SI8 of the Supporting Information.

Single crystals of complexes $Co(Cl_2Gm)_3(Bn\text{-}C_4H_9)_2$, $Co(Cl_2Gm)_3(BF)_2{\cdot}3C_6H_6$, $Co(Cl_2Gm)_3(BF)_2{\cdot}3C_6H_5CH_3$, $\{Co[(n\text{-}C_4H_9S)_2Gm]_3(BC_6H_5)\}_2Co$, $Co\{(n\text{-}C_4H_9S)_2Gm\}_3(BC_6H_5)_2$, and $[(n\text{-}C_4H_9)_4N][Co(Cl_2Gm)_3(BC_6H_5)_2]$ were grown from benzene/heptane, benzene/isooctane, toluene/isooctane, dichloromethane/hexane (1:3 and 1:5) mixtures, and dichloromethane, respectively, at room temperature.

Single-crystal X-ray diffraction experiments were carried out with a Bruker Apex II CCD area detector for the crystals $Co(Cl_2Gm)_3(Bn\text{-}C_4H_9)_2$ and $[(n\text{-}C_4H_9)_4N][Co(Cl_2Gm)_3(BC_6H_5)_2]$ and with a Bruker SMART 1 K CCD area detector for other crystals (graphite-monochromated Mo-K_α radiation, λ = 0.71073 Å, ω scan).[20,21] The substantial redundancy in data allows empirical absorption correction to be applied using multiple measurement of equivalent reflections with the SADABS program.[22] The multitemperature experiment for complex $Co(Cl_2Gm)_3(Bn\text{-}C_4H_9)_2$ was carried out in the temperature range of 30–295 K. Base-centered monoclinic unit cell remains down to 50 K, at which point the structure phase transition begins. This causes the widening of the diffraction peaks followed by the transition to the primitive unit cell with the same crystallographic parameters. At 30 K, the number of systematic absence violation (reflections with the even sum of *h* and *k* indexes) exceeds 56%, and their mean intensity to σ ratio is 6.2. The increase

of temperature up to 40 K caused cracking of the single crystal studied.

The structures were solved by the direct method and refined by full-matrix least-squares against F^2 on all data using SHELXTL software.[23] Non-hydrogen atoms were refined in anisotropic approximation. All *n*-butylsulfide substituents of the molecule $Co\{(n\text{-}C_4H_9S)_2Gm\}_3(BC_6H_5)_2$ are equiprobably disordered over two positions. The C–C bond lengths for the disordered carbon atoms were fixed as 1.53 Å, and anisotropic displacement parameters in two alternative positions were constrained to be equal.

Positions of the hydrogen atoms were calculated and refined using the riding model with isotropic temperature factors $U_{iso} = nU_{eq}(C)$, in which n = 1.5 for methyl groups and 1.2 for the others; U_{eq} values are the equivalent isotropic displacement parameters of the corresponding pivot carbon atoms.

CCDC-773810 (for $Co(Cl_2Gm)_3(Bn\text{-}C_4H_9)_2$ at T = 30 K), -773811 (for $Co(Cl_2Gm)_3(Bn\text{-}C_4H_9)_2$ at T = 60 K), -773812 (for $Co(Cl_2Gm)_3(Bn\text{-}C_4H_9)_2$ at T = 90 K), -773813 (for $Co(Cl_2Gm)_3(Bn\text{-}C_4H_9)_2$ at T = 120 K), -773814 (for $Co(Cl_2Gm)_3(Bn\text{-}C_4H_9)2$ at T = 150 K), -773815 (for $Co(Cl_2Gm)_3(Bn\text{-}C_4H_9)_2$ at T = 180 K), -773816 (for $Co(Cl_2Gm)_3(Bn\text{-}C_4H_9)_2$ at T = 210 K), -773817 (for $Co(Cl_2Gm)_3(Bn\text{-}C_4H_9)_2$ at T = 240 K), -773818 (for $Co(Cl_2Gm)_3(Bn\text{-}C_4H_9)_2$ at T = 295 K), -773819 (for $Co(Cl_2Gm)_3(BF)_2\cdot 3C_6H_6$), -773820 (for $Co(Cl_2Gm)_3(BF)_2\cdot 3C_6H_5CH_3$), -773821 (for $[(n\text{-}C_4H_9)_4N][Co(Cl_2Gm)_3(BC_6H_5)_2]$), -773822 (for $Co\{(n\text{-}C_4H_9S)_2Gm\}_3(BC_6H_5)_2$) and -773823 (for $\{Co[(n\text{-}C_4H_9S)_2Gm]_3(BC_6H_5)\}_2Co$) contain the supplementary crystallographic data for this paper. These data can be obtained free of charge from The Cambridge Crystallographic Data Centre via www.ccdc.cam.ac.uk/data_request/cif.

Supporting Information (see also the footnote on the first page of this article): The details of analytical, spectral, magnetometry, and electrochemical data collections as well as the reagents used and the X-ray diffraction data are given.

Acknowledgments

The authors gratefully acknowledge support of the Russian Foundation for Basic Research (grant nos. 08-03-90107, 09-03-00540, 09-03-90454, 09-03-12231, 09-03-00091, and 10-03-00837), the Council of the President of the Russian Federation for young scientists (grant nos. MK-3161.2010.3 and MK-4268.2010.3), the Federal Agency for Science and Innovation (contract 02.513.12.3098), and the Russian Academy of Sciences (programs 6, 7, 9, and 18).

[1] Y. Z. Voloshin, N. A. Kostromina, R. Krämer, *Clathrochelates: Synthesis, Structure and Properties*, Elsevier, Amsterdam, **2002**.

[2] a) D. R. Boston, N. J. Rose, *J. Am. Chem. Soc.* **1968**, *90*, 6859–6860; b) D. R. Boston, N. J. Rose, *J. Am. Chem. Soc.* **1973**, *95*, 4163–4168; c) R. S. Drago, J. H. Elias, *J. Am. Chem. Soc.* **1977**, *99*, 6570–6577; d) M. A. Murguia, D. Borchardt, S. Wherland, *Inorg. Chem.* **1990**, *29*, 1982–1986; e) Y. Z. Voloshin, N. A. Kostromina, A. Y. Nazarenko, *Teor. Eksp. Khim.* **1990**, *26*, 375–377; f) Y. Z. Voloshin, V. K. Belsky, V. V. Trachevskii, *Polyhedron* **1992**, *11*, 1939–1948; g) Y. Z. Voloshin, V. V. Trachevskii, *J. Coord. Chem.* **1994**, *31*, 147–155; h) S. A. Kubow, K. J. Takeuchi, J. J. Grzybowski, A. J. Jircitano, V. L. Goedken, *Inorg. Chim. Acta* **1996**, *241*, 21–30; i) Y. Z. Voloshin, O. A. Varzatskii, I. I. Vorontsov, M. Y. Antipin, *Angew. Chem. Int. Ed.* **2005**, *44*, 3400–3402.

[3] O. Pantani, S. Naskar, R. Guillot, P. Millet, E. Anxolabéhère-Mallart, A. Aukauloo, *Angew. Chem. Int. Ed.* **2008**, *47*, 9948–9950.

[4] Y. Z. Voloshin, O. A. Varzatskii, T. E. Kron, V. K. Belsky, V. E. Zavodnik, A. V. Palchik, *Inorg. Chem.* **2000**, *39*, 1907–1918.

[5] Y. Z. Voloshin, A. S. Belov, O. A. Varzatskii, A. V. Vologzhanina, S. Viswanathan, J. Radecki, Y. N. Bubnov, *Inorg. Chim. Acta* **2009**, *362*, 2982–2988, and references cited therein.

[6] a) A. Marchaj, A. Bakac, J. H. Espenson, *Inorg. Chem.* **1992**, *31*, 4860–4863; b) A. Bilgin, B. Ertem, F. D. Agin, Y. Gok, S. Karslioglu, *Polyhedron* **2006**, *25*, 3165–3172; c) A. Bilgin, B. Ertem, Y. Gok, *Bull. Chem. Soc. Jpn.* **2007**, *80*, 1549–1555.

[7] Y. Z. Voloshin, O. A. Varzatskii, T. E. Kron, V. K. Belsky, V. E. Zavodnik, N. G. Strizhakova, V. A. Nadtochenko, V. A. Smirnov, *J. Chem. Soc., Dalton Trans.* **2002**, 1203–1211.

[8] Y. Z. Voloshin, V. E. Zavodnik, O. A. Varzatskii, V. K. Belsky, I. I. Vorontsov, M. Y. Antipin, *Inorg. Chim. Acta* **2001**, *321*, 116–134.

[9] a) Y. Kaizu, T. Yazaki, Y. Torii, H. Kobayashi, *Bull. Chem. Soc. Jpn.* **1970**, *43*, 2068–2071; b) Y. Kaizu, Y. Torii, H. Kobayashi, *Bull. Chem. Soc. Jpn.* **1970**, *43*, 3296–3297; c) D. J. Szalda, C. Creutz, D. Mahajan, N. Sutin, *Inorg. Chem.* **1983**, *22*, 2372–2379.

[10] a) H. A. Goodwin, *Top. Curr. Chem.* **2004**, *234*, 23–47; b) R. Sieber, S. Decurtins, H. Stoeckli-Evans, C. Wilson, D. Yufit, J. A. K. Howard, S. C. Capelli, A. Hauser, *Chem. Eur. J.* **2000**, *6*, 361–368; c) I. Krivokapic, M. Zerara, M. L. Daku, A. Vargas, C. Enachescu, C. Ambrus, P. Tregenna-Piggott, N. Amstutz, E. Krausz, A. Hauser, *Coord. Chem. Rev.* **2007**, *251*, 364–378.

[11] Y. Z. Voloshin, O. A. Varzatskii, A. S. Belov, A. V. Vologzhanina, Z. A. Starikova, A. V. Dolganov, V. V. Novikov, *Inorg. Chim. Acta* **2009**, *362*, 5144–5150.

[12] Y. Z. Voloshin, O. A. Varzatskii, A. V. Palchik, E. V. Polshin, Y. A. Maletin, N. G. Strizhakova, *Polyhedron* **1998**, *17*, 4315–4326.

[13] J. R. Pilbrow, *Transition Ion Electron Paramagnetic Resonance*, Calendron Press, Oxford, **1990**.

[14] V. F. Tarasov, G. S. Shakurov, *Appl. Magn. Reson.* **1991**, *2*, 571–576.

[15] F. L. Hirshfeld, *Acta Crystallogr., Sect. A* **1976**, *32*, 239–244.

[16] a) M. Y. Antipin, K. A. Lyssenko, R. Boese, *J. Organomet. Chem.* **1996**, *508*, 259–262; b) K. A. Lyssenko, D. V. Lyubetsky, M. Y. Antipin, *Mendeleev Commun.* **2003**, 60–62.

[17] Y. Z. Voloshin, V. V. Novikov, A. Y. Lebedev, I.E. Paukov, Y. A. Kovalevskaya, *Abstr. IV Int. Conf. High-Spin Molecules and Molecular Magnets*, Ekaterinburg, Russia, **2008**, p. 15.

[18] F. H. Allen, O. Kennard, D. G. Watson, *J. Chem. Soc. Perkin Trans. 2* **1987**, S1–S19.

[19] J. J. Grzybowski, R. D. Alien, J. A. Belinski, K. L. Bieda, T. A. Bish, P. A. Finnegan, M. L. Hartenstein, G. S. Regitz, D. M. Ryalls, M. E. Squires, H. J. Thomas, *Inorg. Chem.* **1993**, *32*, 5266–5272.

[20] Bruker, *APEX2 software package*, Bruker AXS Inc., 5465, East Cheryl Parkway, Madison, WI 5317, **2005**.

[21] Bruker, *SMART*, *Bruker Molecular Analysis Research Tool*, v. 5.059, Bruker AXS, Madison, Wisconsin, USA, **1998**.

[22] G. M. Sheldrick, SADABS, v. 2.01, Bruker/Siemens Area Detector Absorption Correction Program, Bruker AXS, Madison, Wisconsin, USA, **1998**.

[23] G. M. Sheldrick, *SHELXTL*, v. 5.10, *Structure Determination Software Suite*, Bruker AXS, Madison, Wisconsin, USA, **1998**.

Received: April 21, 2010
Published Online: October 29, 2010

